Received: 29 November 2022 | Revised: 25 July 2023 | Accepted: 30 July 2023

DOI: 10.1111/bre.12815

Basin Research | IAS EAGE | WILEY

RESEARCH ARTICLE

Simulations of the effect of smectite-to-illite transition in shales on permeability and overpressures using a stochastic approach, a Norwegian margin case study

Ane Elisabet Lothe[1] | **Arnt Grøver**[1] | **Ole-André Roli**[1] | **Jørn Stenebråten**[1] | **Tron Golder Kristiansen**[2]

[1]Applied Geoscience Department, SINTEF Industry, Trondheim, Norway

[2]Drilling & Wells Department in Drilling Excellence, Aker BP ASA, Stavanger, Norway

Correspondence
Ane Elisabet Lothe, Applied Geoscience Department, SINTEF Industry, P.O. Box 4760 Torgarden, Trondheim NO-7465, Norway.
Email: aneelisabet.lothe@sintef.no

Funding information
Vår Energi, AkerBP ASA, NFR

Abstract

The smectite-illite transition in shales due to subsidence, temperature changes and diagenesis influences many processes in a sedimentary basin that can contribute to overpressure build up like reducing the shale permeability. The smectite-rich layers can form sealing barriers to fluid flows that will influence pore pressure prognosis for drilling campaigns, contribute to sealing caprocks for possible CO_2 storage and to sealing of plugging and abandonment wells. In this work, we have included the diagenetic smectite-illite transition into a three-dimensional pressure simulation model to simulate its effect on pressure build-up due to reduced shale permeabilities over geological time scale. We have also tested effect of thermal history and potassium concentration on the process of smectite-illite transition and the associated smectite-illite correction on permeability. A new smectite-illite correction has been introduced, to mimic how shale permeability will vary dependent on the smectite-illite transition. Stochastic Monte Carlo simulations have been carried out to test the sensitivity of the new correction parameters. Finally, a 3D Monte Carlo pore pressure simulation with 1000 drawings has been carried out on a case study covering Skarv Field, and Dønna Terrace offshore Mid-Norway. The simulated mean overpressures are in range with observed overpressures from exploration wells in the area for the Cretaceous sandy Lysing Formation and for the two Cretaceous Intra Lange Formation sandstones. The simulated smectite content versus depth is in line with published XRD dataset from wells. The corresponding modelled present-day permeabilities for the shales including the smectite-illite transition are two magnitudes higher than measured permeabilities on small samples in the laboratory using transient decay method. The measured permeabilities are in the range of $2.66{\cdot}10^{-18}$ to $3.94{\cdot}10^{-22}\,m^2$ (2695 to 0.39 nD) for the North Sea database and represent the end members for shales-permeabilities with the lowest values, since the small samples are selected with no or minor natural fractures. This work

shows that by upscaling shale permeabilities from mm-scale to km scale, natural fractures and sedimentary heterogeneities will increase the shale permeabilities with a factor of two and that by including permeability correction controlled by the smectite fraction, pressure ramp can be simulated due to diagenesis effect in shales.

KEYWORDS

3D, North Sea, Norwegian margin, permeability measurement, pressure simulations, sedimentary basin, smectite-illite, transition

1 | INTRODUCTION

The smectite-illite reactions are closely related to several processes like hydrocarbon maturation, temperature (Powers, 1967), geo-pressures in shales (Colten-Bradley, 1987; Freed & Peacor, 1989), alternation of fault friction properties (van der Pluijm, 2011), shear stress (Casciello et al., 2011) or microorganisms dissolving smectite (Kim et al., 2004, 2019). The effect of smectite- illite transition can play a role in many sedimentary basins, since it will control pressure buildup above hydrostatic pressures and may also be instrumental for defining pressure ramps (Colten-Bradley, 1987; Lahann & Swarbrick, 2011; Osborne & Swarbrick, 1997). Such pressure ramps defined by smectite-illite transition are described from several sedimentary basins around the world such as Brazparoa and Jidalgo Countries, Texas (Freed & Peacor, 1989), Gulf of Mexico (Harrison & Summa, 1991), from the Gullfaks Area, northern North Sea (Wensaas et al., 1994), Egersund Basin, southern North Sea (Nadeau et al., 2002) and Vøring Basin offshore Norway (Mondol et al., 2008).

The term smectite is used for a group of platy phyllosilicate minerals. Smectite commonly occurs in fine-grained sediments at shallow depths. When the in-situ temperatures range from 70 to 250°C smectite alters to illite (Pytte & Reynolds, 1989). The smectite loses the interlayer water and reacts with K-feldspar to generate illite and authigenic quartz and release water. This can be written as:

$$\text{smectite} + \text{K-feldspar} \rightarrow \text{illite} + \text{quartz} + n\text{H}_2\text{O} \quad (1)$$

Thus, the transition is dependent on the temperature, time and chemical variables. Three different kinetic models of the transformation of smectite to illite (Huang et al., 1993a; Pytte, 1982; Velde & Vasseur, 1992) were compared on four different geological datasets by Crawford Elliott and Matisoff (1996). They concluded that noon of the three models, was successful in all four basins, but that Huang et al. (1993a) gave best simulations results for the Salton Sea and the Gulf Coast. In the basin modelling tool PetroMod, the Pytte and Reynolds (1989) formula for smectite-transformation has been implemented into the compaction model (Hantschel & Kauerauf, 2009), see also Nguyen et al. (2016) for a recent case study using this modelling approach on smectite-rich mudstones offshore Japan. Osborne and Swarbrick (1997) and Swarbrick et al. (2002), on the other hand, suggested simulating smectite hydration as a separate consideration, not as implemented in the compaction model.

Chemical compaction involves the dissolution and precipitation of minerals resulting in reduced porosity and permeability, and increased density. Smectite clays will only compact mechanically to around 40% porosity at about 1.5 to 2 km, this is seen from observations and experiments (Bjørlykke, 1998, 2014; Mondol et al., 2007). At temperatures larger than 70–80°C, smectite is replaced with mixed-layer minerals and illite, and the chemical compaction is dominating (Bjørlykke, 1998). Hence, the heat rate in a sedimentary basin will have an influence on the smectite-illite transition (Huang et al., 1993a). The illitization of smectite generates smaller and stiffer crystals that will influence the mudstone physical properties (Bjørlykke, 1998; Thyberg et al., 2010). The process also reduces the permeabilities to mudstones that may lead to build-up of overpressures (e.g. Bjørlykke & Nadeau, 1998; Freed & Peacor, 1989).

There exist few studies presenting measured permeabilities in lab on natural shales (Daigle & Screaton, 2015; Dewhurst et al., 1999; Hildenbrand et al., 2004; Yang & Aplin, 2007), this is due to large expenses connected to core sampling and the tight rocks results in time-consuming and long experimental campaigns. Mondol et al. (2008) made synthetic mudstones with 100% smectite aggregate as an end member and showed low permeabilities (60 nD at 50 MPa stresses), compared to 0.001 mD using kaolinite aggregates. This is in line with Nooraiepour et al. (2019) that showed a reduction of two orders of magnitude between the permeability of kaolinite- and smectite-rich mixtures using semi-compacted fine-grained sediments in laboratory. The lowest permeabilities were measured using a 15:85 specimens quartz-smectite mixture.

Detection and quantification of abnormal pore pressure in the field is often based on indirect methods like wireline logs (sonic or resistivity to calculate the pressures and gamma-ray to evaluate the lithology). One of the current challenges is to have proper measurement of the assumed pore pressures in these zones, since direct pressure measurements are taken in sandy rich formation using techniques like e.g. repeated formation tests (RFT), formation integrity tests (FIT) or drill stem test (DST). For the shaly overburden, seldom direct measurement is available (for shallow conditions e.g. Strout & Tjelta, 2007), though kick can be an indirect methodology to measure the overpressures.

Drilling operations often rely on local data analogues. When such data are lacking or scare, a good pre-drill model from, e.g. three-dimensional pressure simulator models (e.g. Lothe et al., 2019, 2020) becomes more important. There are several processes contributing to pressure generation in a sedimentary basin like mechanical and chemical compaction, lateral pressure transfer, rapid burial, uplift and erosion. In this work, we present a new methodology on how the smectite-illite transition in shales will influence the permeability to shales dependent on burial depths, and thereby the pressure build-up. We will examine how the shale permeability is dependent on the smectite-illite transition, and how this can be simulated. The uncertainty in the input parameters and resulting simulated shale permeabilities and simulated pore-pressures will be discussed, and the simulation results will be compared with measured shale permeabilities from laboratory work using transient decay method. The new workflow will be tested on a dataset offshore Mid-Norway and compared with measured smectite-illite content using XRD-analysis from two wells in the area, measured permeabilities of shale samples, and measured overpressures from wells in the area. The main research gaps that will be addressed in this article is how the smectite-illite transition will influence the shale permeability, and thereby influence and control the pressure build-up in shales at shallow depths. This knowledge can be crucial when planning explorations wells, but it will also be important to better understand lateral and vertically overburden and caprock properties both for CO_2 storage, energy storage sites or for plugging and abandonment of wells.

1.1 | Geological setting

The study area is situated offshore Mid-Norway, more specifically at the Dønna Terrace located north of Halten Terrace, with Trøndelag Platform to the east (Figure 1a). The 3D simulated study area covers part of the narrow SW–NE trending Dønna Terrace, part of the NW-SE trending Revfallet Fault Complex, and the Sør High to the east (Figure 1b). The Dønna Terrace is deepening towards west, compared to the shallower NW-SE trending Sør High. Jurassic rifting was mapped on platforms and terraces (Blystad et al., 1995), with following post-rift development in Cretaceous (Færseth & Lien, 2002). The Dønna and Halten Terraces are subdivided from the Trøndelag Platform in the Late Cretaceous (Brekke et al., 1999). The shallow units consist of thick shaley deposits of Late Cretaceous to Tertiary age, with some thin sandstone units (Figure 1c). The main sandstone units are the Jurassic Garn Formation, the thin sandstone layers in the dominating shaley Lower Cretaceous Lange Formation, and the sandy Cretaceous Lysing Formation (Figure 1c).

The Late Jurassic syn-rift basin topography was filled during the early Cretaceous post-rift phase with dominantly mud deposits of the lower Lange Formation (Færseth & Lien, 2002). The Cretaceous sand-prone Lysing Formation was deposited during continuous subsiding (Færseth & Lien, 2002). Hansen et al. (2021) have mapped lobe-fringed deposits with channel-fills and channel-lobe transitions, in a post-rift deep-water system.

The Brygge Formation of Early Eocene to Early Miocene age is deposited over most of the Halten Terrace and Dønna Terrace, in a mainly marine environment. On the Halten Terrace, it consists mostly of clay, while out in the Møre and Vøring basin, it consists mostly of ooze deposits (Chand et al., 2011; Eidvin et al., 2007). The fine-grained sediments of the Kai Formation (Middle Miocene to Lower Pliocene) overlie the mid-Miocene unconformity (Eidvin et al., 2007). Depositional environment was generally marine, with sediments deposited on the outer and middle part of the margin. The glaciogenetic Naust Formation was deposited during Pliocene and Pleistocene with thick successions (Rise et al., 2005).

The pore pressures have been measured in the Lower Cretaceous Lange Formation in around 40 wells, defining a regional shale gradient with increasing pore pressures (O'Connor et al., 2008). For well 6507/5-4 at Skarv Field (see Figure 1b), the pore pressure is measured to 140 bar. Below, the Lower and Middle Jurassic reservoirs are laterally drained with overpressures 100 bar lower than the overlying shales (O'Connor et al., 2008). Velocity and density log data from Storvoll et al. (2005), shows low velocity interval in mudstones at the Haltenbanken. For the eastern Haltenbanken, Storvoll et al. (2005) show low velocities observed for the lower Miocene to upper Pliocene Kai Formation and the lower Eocene to lower Miocene Brygge Formation, with an abrupt reduction in the velocities from the overlying Quaternary Naust Formation.

Peltonen et al. (2009) the Late Cretaceous to Early Tertiary sequences of the Vøring and Møre Basins to the

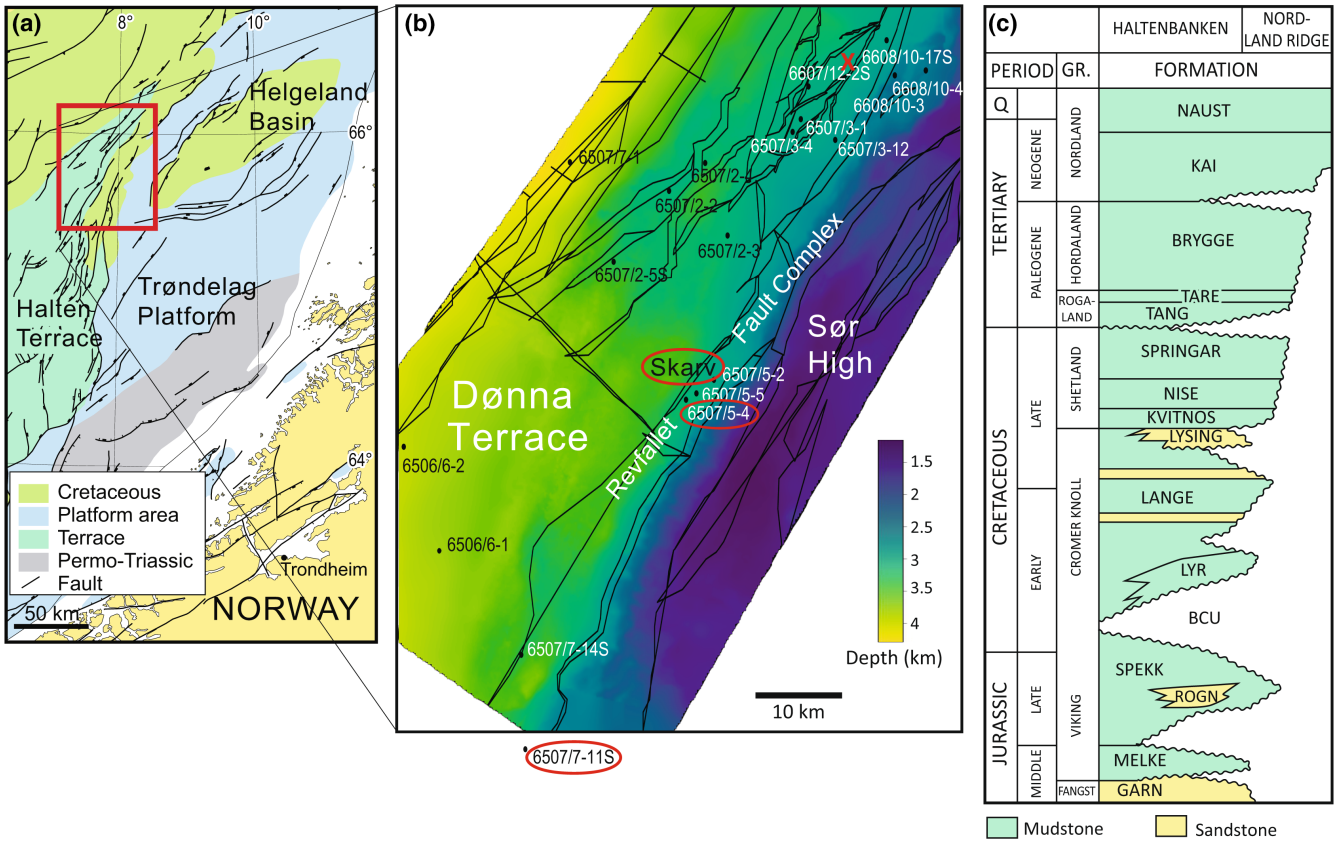

FIGURE 1 (a) Overview map with the study area marked covering Dønna Terrace and Sør High, offshore Mid-Norway. (b) Depth map for the top Cretaceous sandy Intra Lange Formation (S3). Interpreted faults defining pressure compartments and wells with measured pressures used in the study are marked with black and white. Red X marks the pressure compartment used in the result chapter, while red rings mark two wells with XRD data, one outside the study area. Skarv compartment cell is the main studied cell. (c) Simplified lithostratigraphic column from the Halten Terrace and Nordland Ridge, green is dominating mudstone and yellow is dominating sandstone. Reworked from Dalland et al. (1988).

Norwegian Sea, carried out detailed mineralogy studies of cuttings. Using XRD analysis of shales they show progressive alternation of smectite to illite, the same trend as shown by Cicchino et al. (2015) for wells in the Haltenbanken area. Cicchino et al. (2015) also presented geothermal gradients measured from DST temperatures of 40.7°C/km for well 6507/-1 (Alve Field) 6507/5-5 (Skarv Field) that is situated in our study area.

2 | DATA AND MODEL SETUP FOR 3D PRESSURE SIMULATIONS

To set up the 3D geo-model, we had access to 20 interpreted seismic horizons from 2D and 3D seismic surveys covering the study area (Figure 1b), that defines the top of the layers in the geomodel (Table 1). The sand/clay fraction for the layersise defined from sedimentary logs from the area (Table 1). The lithology is predominately shales with four sandstone units; the Cretaceous Lysing Formation, two layers in the Early Cretaceous Lange Formation and the deeper middle Jurassic Garn Formation (Table 1). For the 3D pressure simulations, we assume a constant initial depositional smectite fraction (0.9 of the clay fraction) and potassium content set constant to 0.0035 mol/L for all sediment layers in the model. The paleo-water depths were set constant to 400 m, while today's bathymetry map was used present-day water depth. No erosion or uplift are included in the model set-up.

Leak-off tests (LOT) and formation integrity tests (FIT) from wells in the study area were used to calibrate the input minimum horizontal stress. The input parameters used in the base case are listed in Table 2. For the 3D pressure simulations, the first timestep starts at 161 Ma till the present day, with timesteps of 250,000 years.

2.1 | Datasets used for comparisons

As a part of the workflow, we compared the outcome of the simulations with three independent datasets:

TABLE 1 Overview of input layers used in the simulations.

Layers—Name	Depositional age (Ma)	Water depth (m)	Sand (fraction)	Clay (fraction)	Simulation layer name
Seabed	0.00	Seabed	0.1	0.9	0
Upper Naust Fm	0.02	400	0.1	0.9	1
Top Naust Fm	0.05	400	0.1	0.9	2
Intra Naust Fm	1.5	400	0.1	0.9	3
Kai Fm	4.0	400	0.1	0.9	4
Top Brygge Fm	16.0	400	0.1	0.9	5
Top Tare Fm	55.8	400	0.1	0.9	6
Top Springar Fm	65.5	400	0.1	0.9	7
Shetland Group 2	77.25	400	0.2	0.8	8
Top Lysing S6	89.0	400	0.95	0.05	9
Base Lysing	89.5	400	0.05	0.95	10
Kvitnos Fm S5	90.0	400	0.1	0.9	11
Top Lange Fm S4	93.0	400	0.2	0.8	12
Intra Lange Fm S3	98.0	400	0.95	0.05	13
Intra Lange Fm	99.0	400	0.1	0.9	14
Intra Lange Fm	101.0	400	0.95	0.01	15
Intra Lange Fm S2	103.0	400	0.20	0.8	16
Intra Lange Fm S1	133.0	400	0.1	0.9	17
BCU	138.0	400	0.1	0.9	18
Top Melke Fm	161.0	400	0.1	0.9	19
Top Garn Fm	176.0	400	0.8	0.2	20
Åre Fm	190.0	400	0.1	0.9	21

Note: The sandstone units are marked with gray shades.

- Measured pressure data from exploration wells in the study area
- Published dataset of XRD data from Kvitnos and Lange Formations from two wells in the study area
- Published and own datasets of shale permeabilities from the North Sea and Mid-Norway area

Measured pressures as Formation Integrity Tests (FIT) and Repeated Formation (RFT) tests from sandstone units from exploration wells in the study area are used to check the quality of the simulations.

2.1.1 | XRD datasets

To compare the output of our simulations for the simulated smectite-illite transition, we compare with published XRD analysis by Cicchino et al. (2015) from two wells; wildcat well 6507/7-11S west of Heidrun and 6507/5-4 (Skarv area), see Figure 1 for location. Cicchino et al. (2015) carried out bulk XRD analysis and clay fraction XRD analysis on Cretaceous Lange and Kvitnos Formations with analysis procedures as described in Peltonen et al. (2009) and Cicchino et al. (2015).

In addition, we did our own X-ray diffraction analysis of six shale samples, that were used for shale permeability measurements (Table 3). The smectite and mixed layer content are shown as percent from the bulk rock. The mixed layer represents illite-smectite.

2.1.2 | Shale permeability dataset

We have tested seven shales from the North Sea and the Mid-Norway area using transient decay methods (Table 3), the permeability is measured both vertically and horizontally, and compared with published data (Yang & Aplin, 1998, Hildenbrand et al. (2004).

3 | METHODOLOGY

To illustrate the sensitivity of the model parameters on the transition from smectite to illite, we have set up a range of 1D simulations, where the effect of heat rate, temperature and potassium content have been varied. Thereafter, the smectite-illite transition has been

TABLE 2 Input parameter used in the "base case" without SI transformation included.

Processes	Reference	Parameter description	Symbol		Unit
Lithology "sand"					
Porosity method	Sclater and Christie (1980)	Top porosity		0.49	–
		Bottom porosity		0.03	
			kexp	0.00027	1/m
Permeability	Equation (4) this article	Sand permeability at surface	k0	1.0e-14	m^2
		Permeability exponent	kexp	3.98	
		Density		2300	kg/m^3
		Smectite fraction		0.9	
Lithology "shale"					
Porosity method	Sclater and Christie (1980)	Top porosity		0.63	–
		Bottom porosity		0.01	
			kexp	0.00051	1/m
Permeability	Equation (4) this article	Shale permeability at surface	k0	1.0e-14	m^2
		Permeability exponent	kexp	4.6	
		Density		2650	kg/m^3
		Smectite fraction at surface		0.9	
Smectite-Illite corr.	Huang et al. (1993a)				
		"Turning point" between corr. curves	*SIxs*	0.8	
		Perm. Correction when x = *SIxs*	SIzs	0.001	
		Perm. correction no smectite content	*SIz*0	0.01	
	Huang et al. (1993b) Erratum	Arrhenius factor	A	$8.08*10^4$	Sec^{-1}
		Activation energy	Ea	28	Kcal/mole
		Gas constant	R	1.987	Cal/deg-mole
		Potassium concentration	K^+	0.0035	mol/L
Fault permeability	Borge (2000)				
		Fault width	b	20	m
		Transmissibility (%) remaining at no overlap	tp	0.05	
		Lateral transmissibility	kvert	0.0069	
		Porosity at seabed	Por0	0.48	
		Rate of change in porosity vs. depth	Porc	0.00038	
		Porosity where the K and phi curve changes between shallow and deep relationships	Pors	0.1	m^{-1}
		Permeability where the K-	Port	0.00002	mD
		Rate of change in fault zone permeability for deep faults	Porde	6.0	mDm^{-1}
		Rate of change in fault zone permeability for shallow faults	Porsh	6.0	mDm^{-1}

TABLE 2 (Continued)

Processes	Reference	Parameter description	Symbol		Unit
Temperature gradient model					
		Temperature at sea-level	T0	4	°C
		Thermal gradient	Tgrad	39	°C/km
Stress model	Grauls (1998)				
		Grauls No.		1.147	
Quartz cementation	Walderhaug (1996)				
		Temperature start		80	°C
		Temperature end		175	°C

TABLE 3 Measured vertical and horizontal permeabilities from North Sea and Mid-Norway shales.

Sample	Age	Vsh %	Smectite + mixed layer content (% of bulk rock)	Depth (m TVD)	Permeability vertically (m^2)	Permeability horizontally (m^2)
E	60	64	63.3	1517	809274E-21	329631E-20
T	50	79	39.0	1832	74019E-21	197384E-20
F	40	88	65.0	1857	450233E-19	59081E-18
B2	155	67	47.1	1907	592152E-22	602021E-21
G	55	6	5.00	1976	76733E-19	958023E-18
K	80	56	10.6	2398	394768E-21	407598E-20
C1	166	78	20.9	2923	394768E-22	286207E-21

implemented and tested in three-dimensional pressure simulations, varying the smectite-illite corrections used for the shale permeabilities and varying the temperature gradient for a case study offshore Mid-Norway. Finally, a Monte Carlo approach was carried out, varying several input parameters for 300 and 1000 runs. The simulated shale permeabilities are compared to measured permeabilities in lab experiments using the transient-decay method.

3.1 | Modelling smectite-illite transformation

The smectite-to-illite transformation is modelled using the following kinetic formula from Huang et al. (1993a):

$$-\frac{dS}{dt} = A_{SI} e^{-\frac{E_a}{RT}} [K^+] S^2 \quad (2)$$

where A_{SI} is Arrhenius factor (1/s), E_a is activation energy (cal/mol), $[K^+]$ is potassium concentration (mol/l), R is gas constant (1.987 cal/K mol), S is smectite fraction, t is time (s) and T is temperature (K). A similar model has previously been applied in 1D simulations (Helset et al., 2002). According to this formulation, the temperature is a key factor for the rate of change of smectite, with potassium concentrations serving as a catalyst. The burial history of the sediments and its associated thermal history is there for instrumental in describing the distribution of smectite-illite transformation within a sedimentary basin at present day.

3.2 | 1D smectite-illite transition simulations—Effect of heat rate and potassium content

We have tested implementation of diagenetic effects of the smectite-illite transition in shales in two ways, first by 1D simulations in Matlab, and thereafter in full 3D pressure simulator. In the 1D simulations, the overpressure is not considered.

We are varying the burial history and by that the thermal regime and the potassium content, keeping the other parameters fixed in accordance with Huang et al. (1993a) as shown in Table 2. In these simulations, the whole overburden is not modelled, we are only following one sediment sample.

The simulations represent a sediment sample with initial smectite fraction equals 1 exposed to a selection of four different heating rates (ranging 1–4°C/Myr) over a period of 60 Myr (see Figure 2), each mimicking a sediment

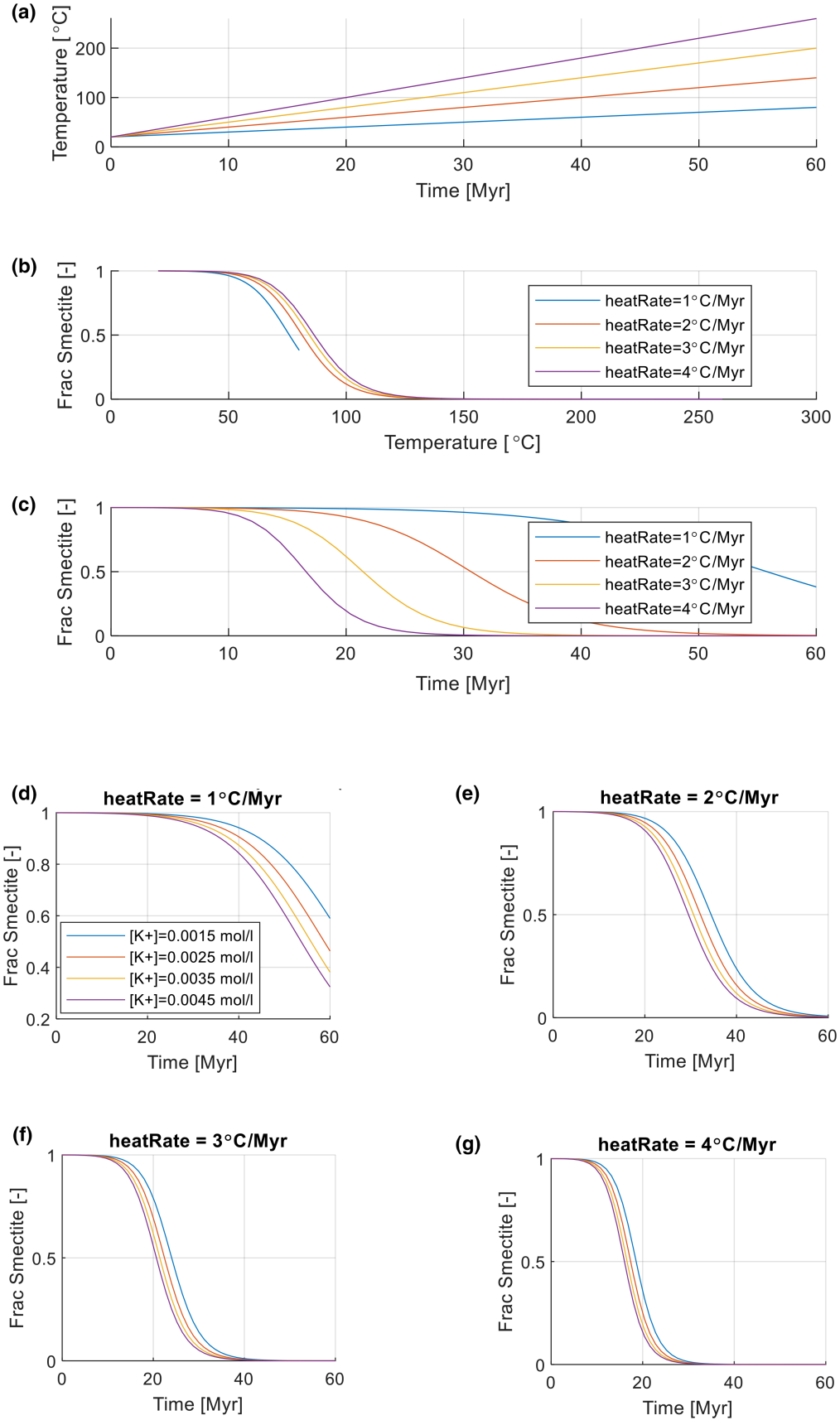

FIGURE 2 (a) Temperature versus time, (b) Fraction smectite content and (c) temperature versus time for different heat rates. The higher the heat rate, the more rapid changes in the smectite content. The potassium content is held constant. Simulated S-I processes versus time varying the heat rates (d) 1°C/Myr, (e) 2°C/Myr (f) 3°C/Myr and (g) 4°C/Myr.

sample buried with a fixed burial rate along a uniform thermal gradient. The temperature (°C) versus time is given as:

$$T(t) = T_0 + heatRate \bullet t \quad (3)$$

where T_0 is surface temperature (°C), t is time (million years), and heatRate (°C/Myr). The surface temperature was kept fixed at 20°C.

Figure 2a–c show smectite fraction transition versus time and temperature varying the heating rate, with potassium content set constant to [K+] =0.0035 mol/L. With a heating rate of 1°C/Myr, the sample reaches 80°Cs at end of simulation (after 60 million years), corresponding to a burial depth of 1500 m (with a burial rate of 25 m/Myr). A heating of rate of 2°C/Myr, the sample reaches the same depth/temperature at half of the time (30 million years, see Figure 2a). The smectite percentage has been reduced to 38% for the first case after 60 million years, while for heating rate of 2°C/Myr, similar smectite fraction is reached after 33 million years and completely converted about 55 million years after deposition (Figure 2b).

The simulations show that with a higher heating rate, the more rapid the smectite fraction will be reduced (Figure 2c). Naturally, the smectite-illite transition will be controlled by the temperature, with less and slower alternation with colder temperatures in a basin and we see from Figure 2b, that the smectite-illite transition stops with low temperatures and low heat rate (1°C/Myr). Figure 2d shows the effect of varying the potassium content in Equation 1, where increased potassium content will increase the smectite fraction effect. The effect of the potassium content is larger at low rates (Figure 2d), compared to higher heat rates (Figure 2e–g).

3.3 | 1D calculating initial smectite fraction from observed XRD clay fraction

We have used the observed XRD fractions from the two wells to back-calculate to the initial smectite fraction. First, the pressure compartment for the well locations was located. The sub-layers used in the original geo-model that match the present-day sample depths were used as proxy for modelling the smectite-illite transition. The associated burial history of the sample locations was calculated. Then, forward simulations of the smectite-illite transformation using a kinetic model by Huang et al. (1993a) were carried out for each sample. For the thermal history, the surface temperature was set to 4°C, and the thermal gradient to 40°C/km uniformly through the geological history. The goal is to find the initial smectite content that best matches the measured present smectite fraction (samples). We used a search algorithm with initial smectite fractions (at deposition), that will search until the modelled smectite fraction matches observed smectite fraction within an error tolerance of 0.001.

3.4 | Methodology—3D pore pressure simulations

The Pressim2.0 software (Grøver et al., 2018; Lothe et al., 2020, 2022) is a 3D pressure simulator, using a restored sedimentary basin history as input, where the main timesteps are defined from interpreted seismic horizons from the study area, both for the overburden (e.g. often shales or chalk) and reservoir units (often sandstone layers). The simulator is customized to model pore-water pressure generation and dissipation in 3D over geological time scales. The simulator has been rewritten in the last years (Grøver et al., 2018, Lothe et al., 2020, 2022), but the simulator is still built on the same basin modelling principles as presented in Borge (2000) and Lothe (2004). The basic assumption is that the fluid flow dynamics can be described by pressure compartments, that is defined by interpreted faults at a given depth, usually at top reservoir level. The faults are assumed to be vertical, and if the pressure compartments vary dramatically in depths, "pseudo-faults" with no throw are included (Lothe et al., 2004). The change in porosity is given by empirical depth-dependent compaction curves for the different lithologies (Sclater & Christie, 1980), and kinetic equations reflecting the degree of chemical compaction (e.g. effect of quartz cementation in the sandstone units using model by Walderhaug (1996)). The tool quantifies pressure dissipation using a model for lateral cross-fault fluid flow (Borge & Sylta, 1998) and Darcy flow equations in the vertical direction. The Griffith-Coulomb failure and the frictional sliding criterion are used to simulate hydraulic leakage from the overpressured compartments (Lothe et al., 2004). The overburden weight and minimum horizontal stress are treated as principal stresses. The minimum horizontal stress is given by an empirical function introduced by Grauls (1998). The minimum horizontal stress was calibrated to leak off test data from wells in the study area.

A thermal gradient model is included for calculating the temperature at a given depth within the basin at a given time step, by assigning surface temperature and thermal gradient within the basin at each geological time step. The simulations start at deposition of the lowest reservoir unit and simulate pressure generation and dissipation in forward manner till the present day. The input parameters such as shale permeabilities are varied, so that the simulated overpressure should match the measured pore pressures from different pressure compartments with different wells in the area.

3.5 | Effect of smectite-illite on pressure model: Permeability alterations

Diagenetic reactions in shales, such as smectite-illitization, changes the microstructure of the shale (Bjørlykke & Nadeau, 1998; Hower et al., 1976; Nadeau & Reynolds, 1981). The flow properties, and thus also the permeability, are therefore affected by shale diagenesis. Similar arguments can also be made for pore space alterations, which can impact the pressure generation within the sediment. A simple approach to combine these effects is by introducing a correction factor to the shale permeability depending on the smectite-illite content fraction. The sediment permeability is calculated using a variant of porosity-permeability relationship often used in basin models (see also Yang & Aplin, 1998):

$$k = k_0 \left(\frac{e}{e_0} \right)^{\text{kexp}} \tag{4}$$

where k_0 (m^2) is the sediment permeability at surface, kexp is the permeability exponent, e is void ratio (pore volume divided by sediment volume) and e_0 is void ratio at surface. Each lithology is defined with its own set of k_0 and kexp, as listed in Table 2. The bulk permeability is calculated as an average over the mix of sediment lithologies (e.g. fraction of sand, clay and carbonates) (see also Table 1 for fraction distribution for the input layers).

The correction factor to the permeability calculated by Equation (2) is given by:

$$k_{corr} = kC_s \tag{5}$$

where C_s is the correction factor related to the state of smectite-illitization. The permeability correction is controlled by the smectite-illite reaction progress. It has been suggested (Bjørlykke & Nadeau, 1998) that permeability reaches a minimum ("turning point") early in the reaction when there is a mixture of smectite and illite particles in the system (see Figure 3a). Bjørlykke and Nadeau (1998) observed that the permeabilities were reduced by several orders of magnitudes, by temperatures of 150°C, due to illite formations in sandstones from the Norwegian Continental Shelf. In the simulations, we have included a correction factor depending on smectite fraction, and that is defined by three curve parameters. The correction parameters are named as shown in Figure 3b:

- *SIxs* = "Turning point" between the two correction curves, at smectite fraction x
- *SIzs* = permeability correction (max impact) when smectite fraction x = *SI_xs*
- *SIz0* = permeability correction with no smectite content.

The permeability correction factor is implemented with two relationships (Figure 3b):

$$C_s(x) = \begin{cases} 10^{\left(SIz0 + \left(\frac{SIzs - SIz0}{SIxs}\right)x\right)}, & 0 < x < SIxs \\ 10^{\left(-\left(\frac{-SIzs}{1-SIxs}\right) + \left(\frac{-SIzs}{1-SIxs}\right)x\right)}, & SIxs < x < 1 \end{cases} \tag{6}$$

where x is the calculated fraction of smectite at a given time-step in the simulations, and x is ranging between 0 and 1. For instance, if one assumes a smectite content of 0.9 of the clay fraction, this will correspond to a correction factor in range of 10^{-2} using the input parameters illustrated in Figure 3b.

At each simulation time step the degree of compaction in the basin is calculated (porosity update) due to incremental sediment load and temperature effects, impacting in-situ pressure generation. In parallel, the degree of smectite-illite transformation is calculated following the kinetic equation by Huang et al. (1993a, 1993b Eq. 2) depending on given burial depth and temperature regime during time step. The resulting overpressure within the time step is again coupled with the dissipating pressure capability (shale permeability) as described above. Hence, the smectite fraction at given time step impact the correction and the pressure dissipating capabilities.

The simulation workflow is presented in Figure 4, with the smectite content is simulated, varying

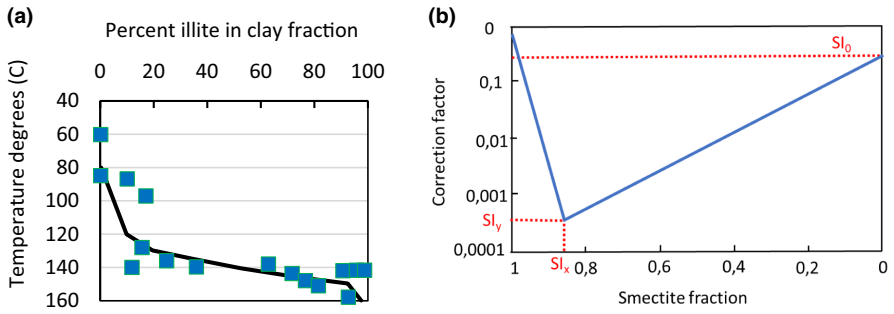

FIGURE 3 (a) Temperature plot of sandstone diagenetic illite contents within the clay fraction, determined from X-ray diffraction from NCS, reworked from Bjørlykke and Nadeau (1998), (b) Example of correction factor plotted versus smectite content (fraction) used in the simulations. Parameters marked in red.

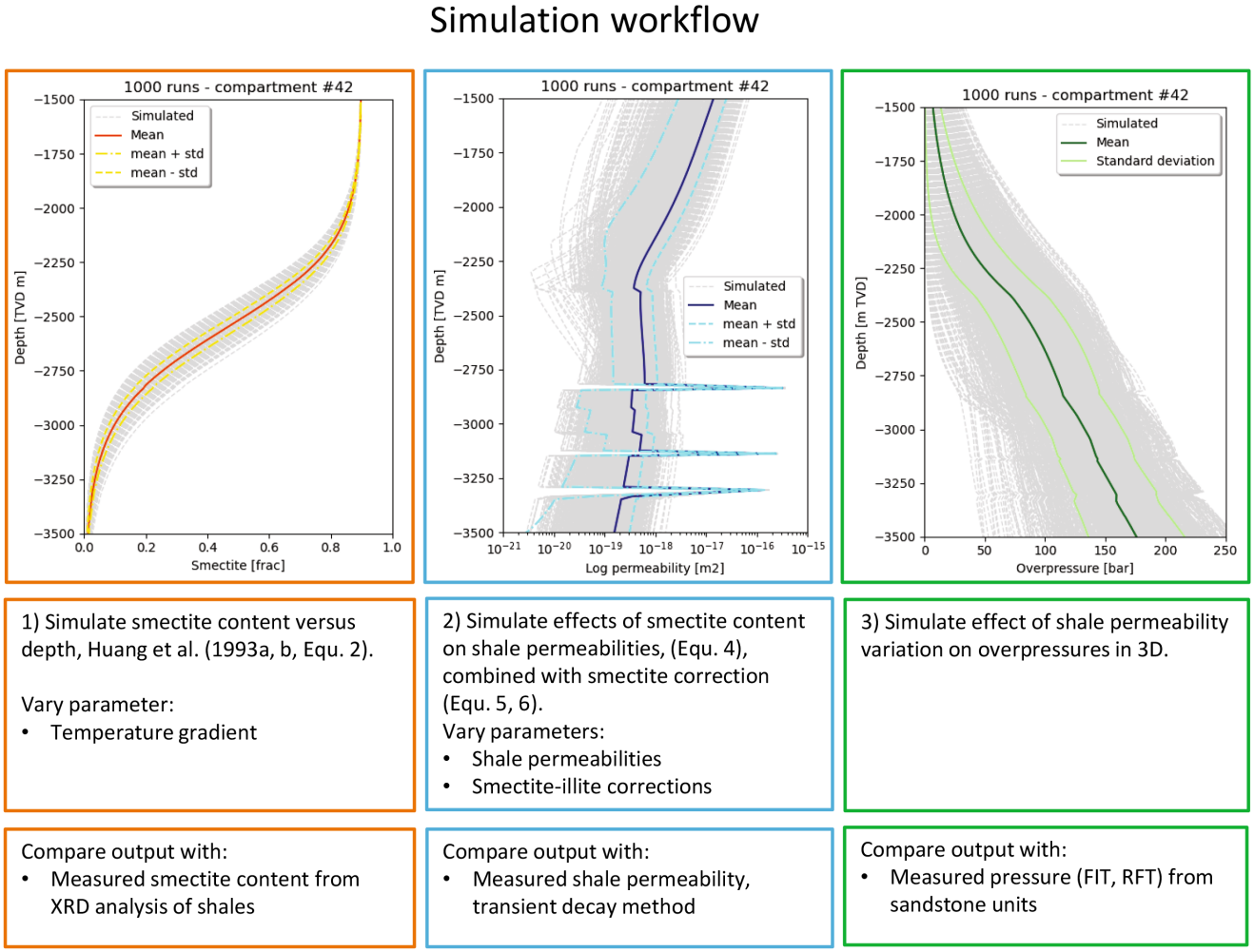

FIGURE 4 Simplified simulation workflow with varied parameters and comparison to measured data shown. Examples of (1) simulated smectite fraction versus depth, (2) permeability versus depth and (3) simulated overpressures versus depth for a pressure compartment.

temperature gradient, the shale permeability is calculated, and the smectite effect is implemented as described above. The simulated shale permeability can be compared with permeability shale measurements but is to calibrate to the measured shale permeabilities. Finally, the simulated 3D overpressures can be compared with measured overpressures in sandstone units from exploration wells in the area.

3.6 | Monte Carlo methodology

The Monte Carlo technique consists of generating a range of different outcomes when the potential for random variables is present. In general, a pitfall in the basin simulators is the vast number of input parameters, their inherent uncertainty, as well as the uncertainty of the model process itself. Several simulation input realizations may give same fits to observation data, hence the question of objectivity of the predictions is often the case. The model input parameters listed in Table 2 for the pressure simulation can technically be treated as stochastic variables following a given probabilistic distribution (normal and uniform) with an associated mean and a standard deviation. However, in this article, we have only varied the input parameters presented in Table 4.

The Pressim2.0 simulator is in principle a deterministic simulator with a fixed set of deterministic input parameters, but by running multiple simulations/realizations in a Monte Carlo scheme, each run with random picks for each of these input parameters drawn from its associate probabilistic distribution, a probability distribution of the calculated overpressures is made. The input section provides information on which sets of input parameters that are treated stochastically in presented case studies (see overview in Table 4). There is no weighting of the simulated pore pressures in the present simulations.

TABLE 4 Overview of simulations runs, with parameter setup and parameter variations.

	Parameter	*Distribution*	*Mean*	*Dev. Max. Width*	*Unit*
Case 1 (base case), deterministic run, without smectite-illite transition					
	–	–	–	–	
Case 2, deterministic run, With smectite-illite correction					
	SIxs		0.8		
	SIzs		0.01		
	SIz0		0.1		
Case 3, Monte -Carlo, 300 runs					
Smectite-illite correction	*SIxs*	Gaussian	0.8	0.08	
Case 4, Monte Carlo, 300 runs					
Smectite-illite correction	*SIzs*	Uniform	0.1	0.001	
Case 5, Monte-Carlo, 300 runs					
Smectite-illite correction	*SIz0*	Uniform	1.0	0.01	
Case 6, Monte-Carlo, 300 runs					
Smectite-illite correction	*SIxs*	Gaussian	0.8	0.08	
	SIzs	Uniform	0.1	0.001	
	SIz0	Uniform	1.0	0.01	
Case 7, Monte-Carlo, 300 runs					
Temperature gradient	Tgrad	Gaussian	40	1	°C
Case 8, Monte-Carlo, 1000 runs					
Temperature gradient	Tgrad	Gaussian	40	1	°C
Permeability shale	ko	Gaussian	1.0e-14	1.0e-15	m^2
	kexp	Gaussian	4.6	0.3	
Smectite-illite correction	*SIxs*	Gaussian	0.8	0.08	
	SIzs	Uniform	0.1	0.001	
	SIz0	Uniform	1.0	0.01	

Note: The colours are used to distinguish between deterministic (light orange) and stochastic (dark orange) simulation runs.

3.7 | Simulation runs set-up

The deterministic simulation cases are split into two cases: case 1 (base case) and case 2 which, respectively does not and does includes the permeability correction due to smectite-illite transformation described in the methodology chapter, and six stochastic simulation cases (Monte Carlo simulations). For Cases 3, 4 and 5; input parameters linked to the smectite-illite transformation are varied stochastically (Table 3), while the remaining input parameters are kept constant at in the base care (Table 2). For Case 6 all three parameters linked to the smectite-illite transition are varied for 300 runs. For case 7, only the thermal gradient is varied, keeping the smectite-illite transition parameters constant. Case 8 presents a larger simulation run with 1000 realizations, varying temperature gradients, smectite-illite correction and shale permeability parameters. The stochastic input distributions for Monte-Carlo simulations are listed in Table 3. Notice that in case 8 with 1000 realizations, also the shale permeability at surface (k_0) and permeability exponent (c) in Equation 4 is varied (see Table 4).

Model input parameters for the deterministic base case are listed in Table 2. This includes the mechanical compaction curve parameters and quartz cementation for porosity alterations for the defined lithologies, associated permeability parameters, as well as flow parameters for fault transmissibility calculations. In all cases, we have used a uniform surface temperature and a uniform thermal gradient for all geological time steps.

3.8 | XRD analysis

The mineralogical composition of representative parts of the two shale samples was determined by qualitative and semi-quantitative X-ray diffraction analysis, whole rock and fine fraction <4 μm.

For whole rock (bulk) analysis representative samples at about 2.5 grams were ground in an agate mortar until all solid particles were in the silt fraction or finer. The samples were then dried at room temperature (20°C) and mounted as unoriented powder on sample holders. Samples for fine-fraction analysis were left in de-ionized water overnight and disaggregated by gently stirring with a glass rod and treatment with an ultrasonic vibrator. The fine fraction <4 μm was separated by settling (according to Stokes law) in 500 mL glass cylinders containing de-ionized water, collected on millipore filters (oriented samples) and treated with $MgCl_2$, and at last inverted onto discs made of quartz glass. Each mineral has characteristic reflections on the X-ray diffractogram and can therefore be identified. The sample preparations were analysed with a Philips PW1710-based X-ray diffractometer with spinner and automatic sample changer at the following conditions: Range (2θ): 2°–52° (2°–35° for fine-fraction), radiation is monochromatic CuK_{α}, voltage is 40 kV, current is 30 mA and speed 1°/minute. The fine fraction was analysed both dry and after saturation with ethylene glycol. The mineralogical composition was determined by the interpretation of characteristic reflections on the X-ray diffractogram. The quantification of each mineral was based on the product of the peak area (the peak height multiplied by the peak width measured at half the peak height) and a weighed factor (relative to quartz).

3.9 | Methodology for permeability measurements

Due to their inherent low permeability, standard methods are usually not used for shales. Two alternatives exist: one can either estimate the permeability indirectly from consolidation experiments or use a direct calculation from transient experiments, where a sudden pore pressure difference is established on opposite sides of a thin disk-shaped specimen and the pressure decay back to equilibrium is analysed. An advantage of the transient method is that the measurements are performed with small pressure perturbations. It is then valid to assume linearity in all relations and to neglect surface effects. This greatly simplifies the analysis.

The permeability measurements are carried out in the SINTEF formation physics lab and are performed under isotropic external pressure with fluid pore pressure at room temperature. The transient decay method is used (see also Horsrud et al., 1998), and the test is performed twice for each sample with a reversal of the pressure amplitude. The average of the two measurements per sample is used to calculate the permeability. All tests are performed at the same isotropic confining pressure of 16.0 MPa and a pore pressure of 10.0 MPa with 0.5 MPa pore pressure amplitude for the decay measurements. A brine (3.5 wt. % NaCl) is used during the testing to relieve capillary suction on the sample surface and establish pore pressure communication. A schematic of the test setup, consisting of the pressure vessel and the end pistons with the mounted sample, is presented in Figure 4.

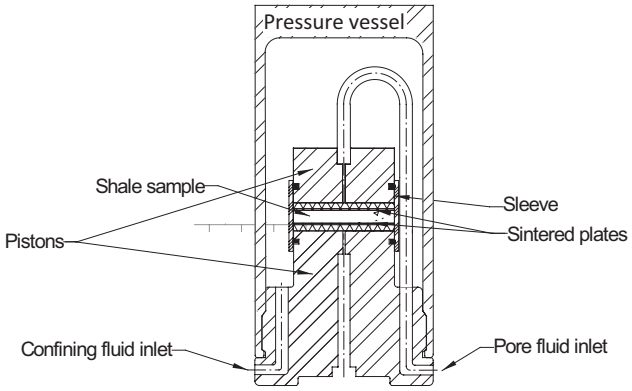

FIGURE 5 Schematic drawing of the cell used to measure permeability on shale thin discs under confinement pressure.

The sample is a cylindrical, disk-shaped sample with nominal diameter of 38.1 mm and is mounted between two steel pistons and sintered disks, with a rubber sleeve around the cylindrical surface. The thickness of the samples ranged from 10 to 20 mm. The sample is exposed to a confining pressure through the sleeve and pistons (see Figure 5). At the end surfaces of the sample, pore fluid may enter or escape through two sintered steel disks. Confining and pore pressure are applied to the sample, which is allowed to consolidate. After consolidation, a pore pressure difference is generated across the sample by two needle valves and the ensuing evolution of the differential pressure is measured with a differential pressure transducer. The two sides of the sample are each connected to a pressure accumulator and a pump through ball valves, which give the least pressure change during closing. The confining pressure is generated by a pump and an accumulator keeps the pressure constant.

All samples were prepared parallel or perpendicular to the sediment layers. The sample extraction was performed with a rotary core barrel, end-cutting was performed with a masonry saw with diamond-impregnated cutting surface, and the end-preparation was performed by wet-grinding using a 320-grit paper. An inert laboratory-grade oil (Marcol 82) was used during preparation to prevent any change in the natural fluid content, and act as a circulation- and cooling fluid. Following preparation and prior to testing the samples were stored submerged in Marcol 82 in closed containers.

4 | RESULTS

First, we carried out deterministic runs with and without permeability corrections. Thereafter, several Monte-Carlo stochastic simulations were carried out, varying input parameters as shown in Table 2. The output of the simulations were compared with measured datasets for smectite content, shale permeability and overpressures.

4.1 | 3D pressure simulations—Simulations without (case 1) and with permeability correction (Case 2)

For the 3D deterministic pressure simulations, we assume a constant smectite fraction versus depth for the whole study area (Figure 6a). Figure 6b shows a comparison for one pressure cell (see Figure 1b, red x) between base case keeping all the input parameters constant as shown in Table 2, only varying without (case 1) and with (case 2) the smectite-illite effect on calculated permeabilities versus depth. The simulations show a reduction in the shale permeabilities along the whole sedimentary column in order of two magnitudes, with the largest reduction in the permeabilities around 2.2 km depths. The thin sandstone layers can be observed as four "peaks" with higher permeabilities. Figure 6c shows the corresponding simulated present-day overpressure build up for the same pressure compartment, using this two permeabilities with and without the effect of smectite-illite transition included. By introducing the smectite-illite transition correction on the shale permeability, a shallow pressure build-up starting from around 1.8 km to 2.2 km are simulated.

4.2 | Monte-Carlo simulations—Vary smectite-illite correction (cases 3, 4, 5 and 6)

Thereafter, we varied the three input parameters controlling the smectite-illite correction on the permeability *SIxs, SIzs* and *SIz*0. For each input parameter we performed 300 runs, keeping the rest of input parameters constant, for pressure cell X at Figure 1 (Figure 7, Tables 2 and 3). For parameter *SIxs* a Gaussian distribution was selected, since the Bjørlykke and Nadeau (1998) article indicated a larger impact around the "turning point" (see Figure 3a with rapid increase in illite fraction due to increased temperatures), while *SIzs* and *SIz*0 is set up with a uniform distribution (Figure 7a–c).

First, the "turning point" of the smectite-illite correction was varied by changing parameter Six following a Gaussian distribution with mean 0.8 and standard deviation 0.2 (Figure 7a, case 3), this has the largest effect on the

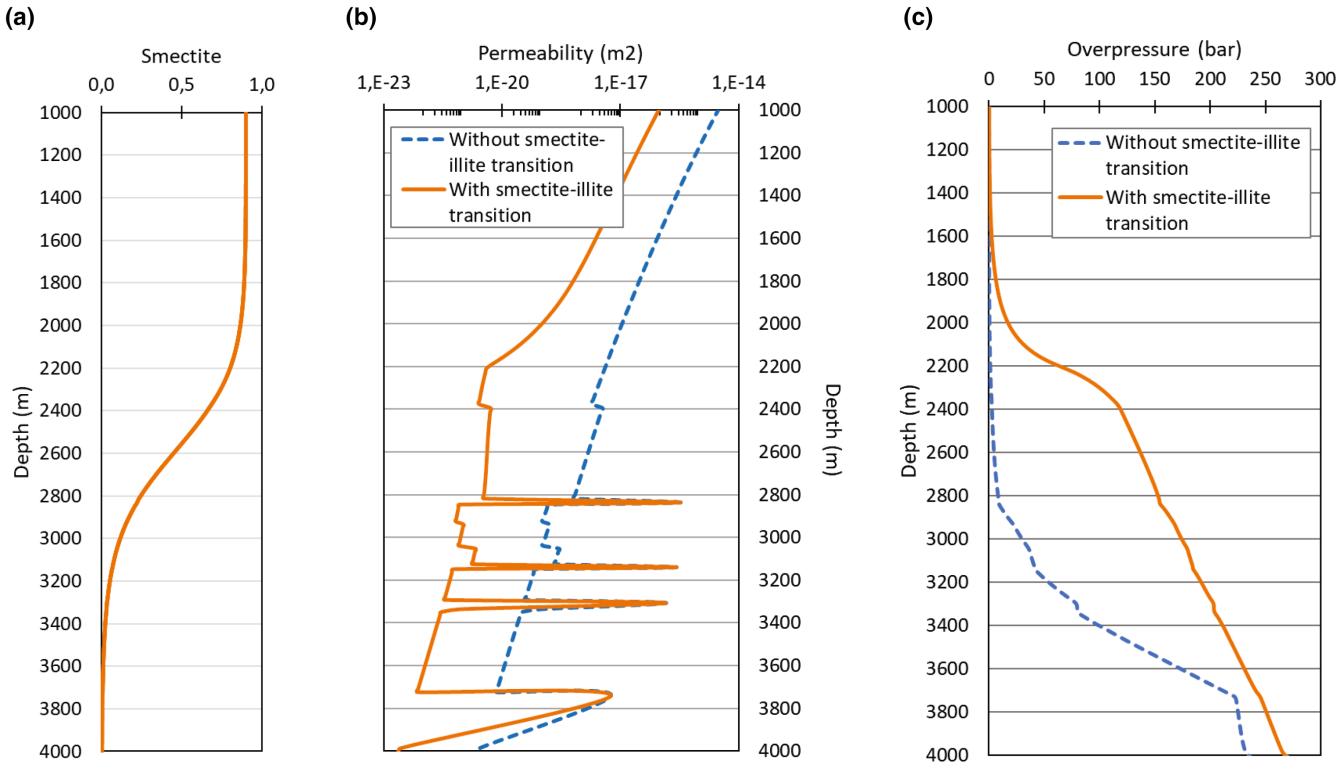

FIGURE 6 (a) Simulated smectite content versus depth TVDm for a sediment column (pressure cell marked with red X in Figure 1), (b) calculated permeabilities without and with including effect of smectite-illite transition versus depth for the same pressure cell, (c) Simulated overpressures (bar) versus depth only varying the permeabilities with and without S-I transition effects.

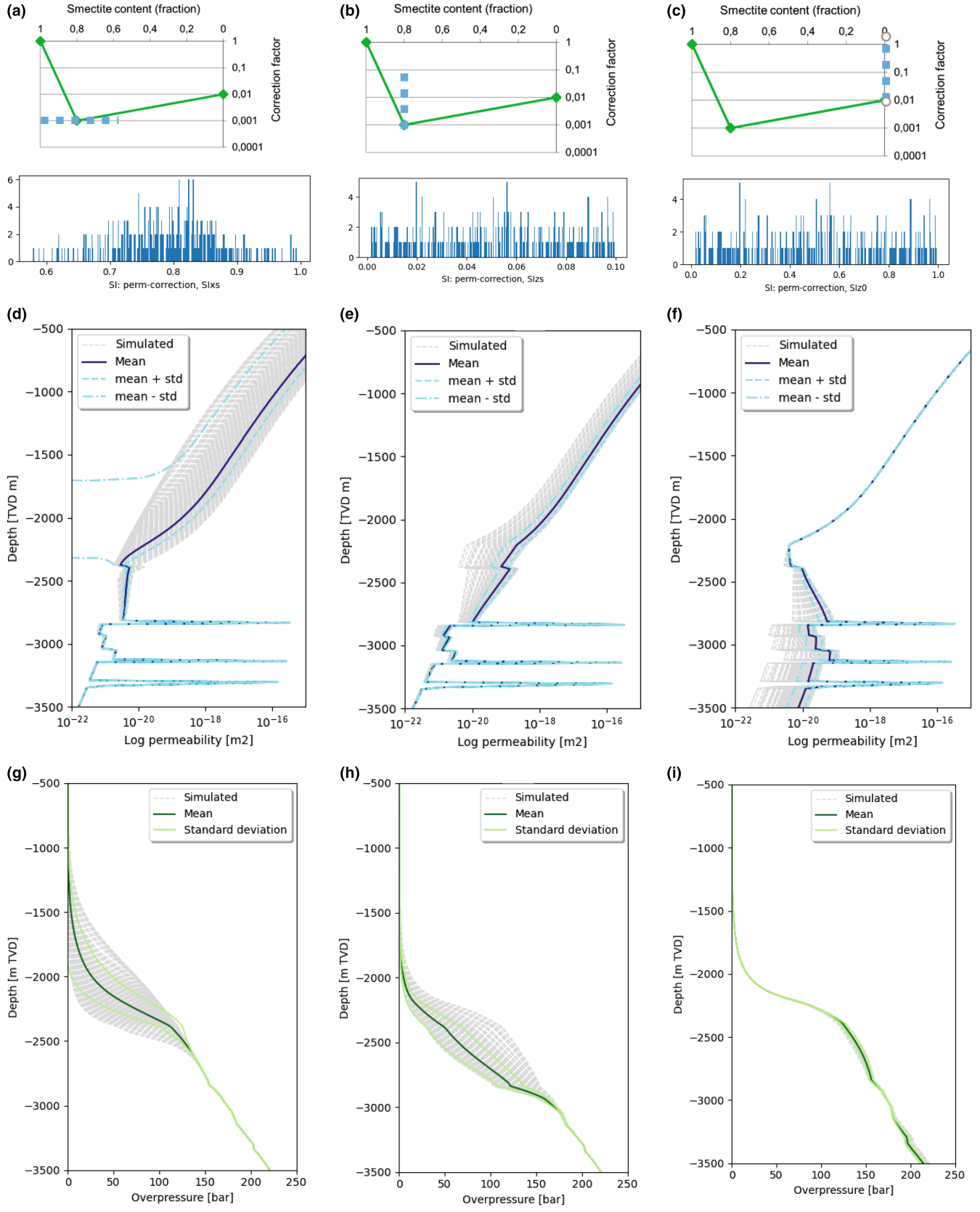

FIGURE 7 Monte Carlos simulations varying SI corrections for permeability as input to 300 runs for: (a) vary *SIxs* with Gaussian distribution 0.8 ± 0.2, with resulting (d) permeability (m^2) versus depth (m) and (g) simulated overpressure (bar) for one compartment. (b) Uniform distribution of parameter *SIzs* used 300 runs results in (e) simulated permeability and (h) simulated overpressure for the same compartment. (c) Input *SIz*0 with uniform distribution result in (f) permeability and (i) simulated overpressures.

permeabilities at shallow depths <2.3 km (Figure 7d). The reduced permeability for the shales resulted in simulated shallow pressure build ups, in this case starting from approximately 1.5 km (Figure 7g). Varying parameters *SIzs* with uniform distribution between 0.1 and 0.001 reduces the shale permeability in the shallow part, and around a "breaking point" at 2300 m depth (Figure 7b,e, case 4). This results in a varying pressure build-ups starting from 2 km depth, with the highest ramp build-up around 2.3 km m depth (Figure 7h). Varying the SI correction parameter *SIz*0 uniformly from 0.01 to 1 results in reduced permeability at depth >2.4 km, thus the corresponding simulated overpressures have minor variation in magnitude (Figure 7c,f,i, case 5).

When we vary all the three SI parameters in the same runs (case 6, Table 2), we observe a decrease in the simulated permeabilities for the shales along the whole depth interval, with a ramp structure around 2300–2500 m depth (Figure 8a). The reduced permeability results in simulated increased overpressure versus depth in the compartment (Figure 8b).

4.3 | Varying the temperature gradient (case 7)

The temperature gradients are varied with Gaussian distribution with mean and standard deviation: 40 ± 2°C for the study area, with the rest of the parameters kept constant as in Table 2. Varying the temperature gradients (Figure 9a), have influence on the smectite-illite transition with initial value of 0.9, and increased illite fraction starting from approximately 1.5 km (Figure 9b). This will have some influence on the simulated shale permeability below 2.0 km to 2.3 km and will therefor also influence overpressure build-up in a restricted depth interval (Figure 9c,d). At depths larger than 2.5 km, there is simulated no effect on the overpressure (Figure 9d).

4.4 | Monte-Carlo simulations varying several input parameters for 1000 runs (case 8)

A large simulation case, with thousand Monte Carlo drawings, were set up varying six parameters defining the smectite-illite transition, the shale permeability, and the temperature gradient, keeping the rest of the input parameters constant (Tables 4 and 2). The resulting simulated present-day mean overpressures from the 1000 simulations, can be plotted in map view for the Lysing Formation, and the two deeper sandstone units in Lange Formation (Figure 10a–c). We have not used any weighting, of the Monte Carlo runs, only compared the simulated mean porepressures with measured porepressures from exploration wells in the area.

For Lysing Fm. hydrostatic to very low overpressure (< 40 bar) is simulated along the Revfallet Fault Complex, with low overpressures in the Dønna Terrace area (Figure 10a). Thus, if we map the deviation between mean Monte Carlo modelled and measured overpressures, we see for Lysing Formation around 20–30 bar to large overpressures simulated in the Dønna Terrace area, but with no or very little deviation in the northern part of the study area. The pressure cells with no data for measured pressures are without colour in Figure 10d–f.

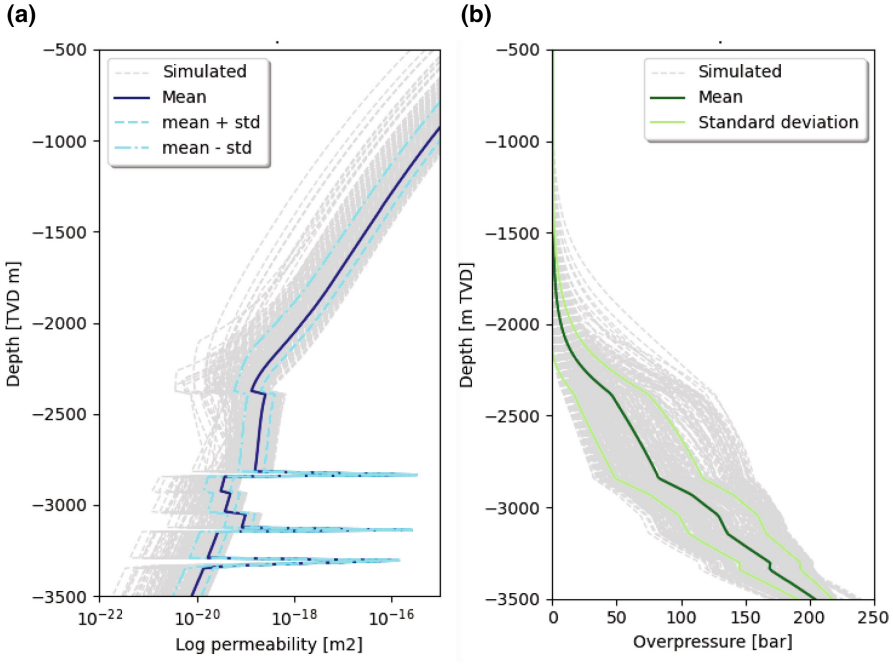

FIGURE 8 (a) Simulated permeability varying the three SI input parameters for 300 runs, (b) Simulated overpressures using the simulated shale permeability for shales. The other parameters are kept constant.

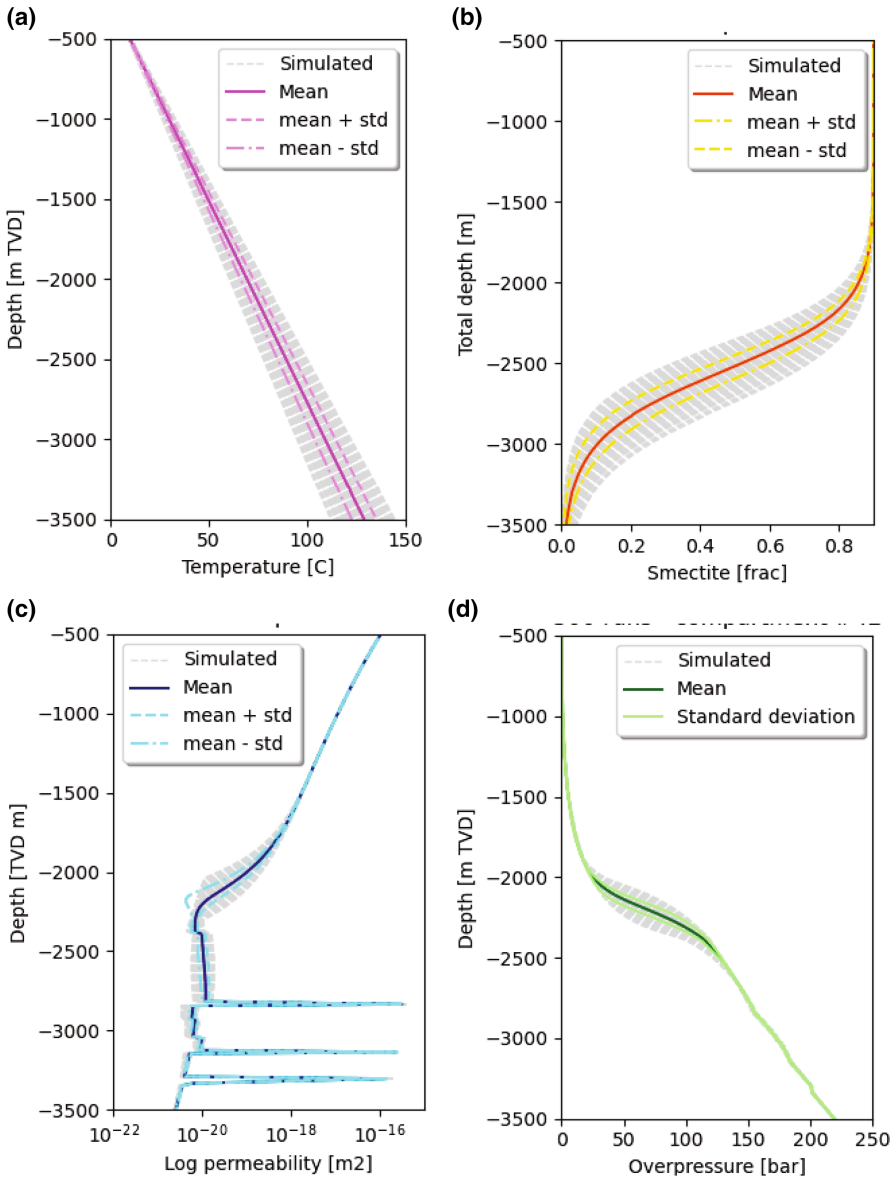

FIGURE 9 300 simulation runs varying (a) the input temperature gradient versus depth with Gaussian distribution mean 40 ± 2°C, (b) Corresponding simulated smectite fraction versus depth, (c) Simulated log permeabilities for the sediment column and (d) Corresponding simulated overpressures (bar)versus depth (m) with mean and one standard deviation for the same pressure compartment.

For the sandstone layers in the Lange Formation, the lowest overpressure is simulated up in the north-eastern part of the study area with around 50 bar, while in the main parts, the simulated overpressure is around 150 to 200 bar (Figure 10b,c). Plotting the deviation maps between mean simulated overpressure and observed overpressure for the two sandstone units in Lange Formation, we see very good match in the northern Alve area and in the Skarv area, with deviation <10 bar.

Figure 11 shows the simulated present-day shale and sandstone permeabilities versus depth in the pressure compartment defined for the Skarv field (see Figure 1 for location). The different runs are shown in grey, with the mean permeability with one standard deviation shown. The mean permeability is gradually reduced versus depth till around 2400 m depth, while there is a "break point" around 2200 m, especially seen for the lowermost standard deviation (Figure 11a). Below, the simulated permeabilities are reduced, but with lower rate. At 2400 m depth, the simulated shale permeabilities varies in range from 1e-18 m^2 to 1e-20 m^2. The vertically measured permeabilities have lower magnitude, compared to horizontally measured permeabilities for all samples. The permeabilities in the sandstone units, have not been varied, and can be seen as "spikes" with higher permeabilities than the shales.

If we compare the simulated shale permeabilities with measured permeabilities on North Sea shales using transient decay method, carried out vertically and horizontal to the shale layers, we observe that the simulated permeabilities is one to two orders of magnitude higher that the measured permeabilities (Figure 11a). We see that the shallow shale samples, from <2 km depth, have smectite + mixed layers from 47% to 65% of bulk rock with vertical low permeabilities (Figure 11a). One sample, from 1976 m depth, has very little smectite and mixed layer content (5%), compared to the other samples at shallow depths.

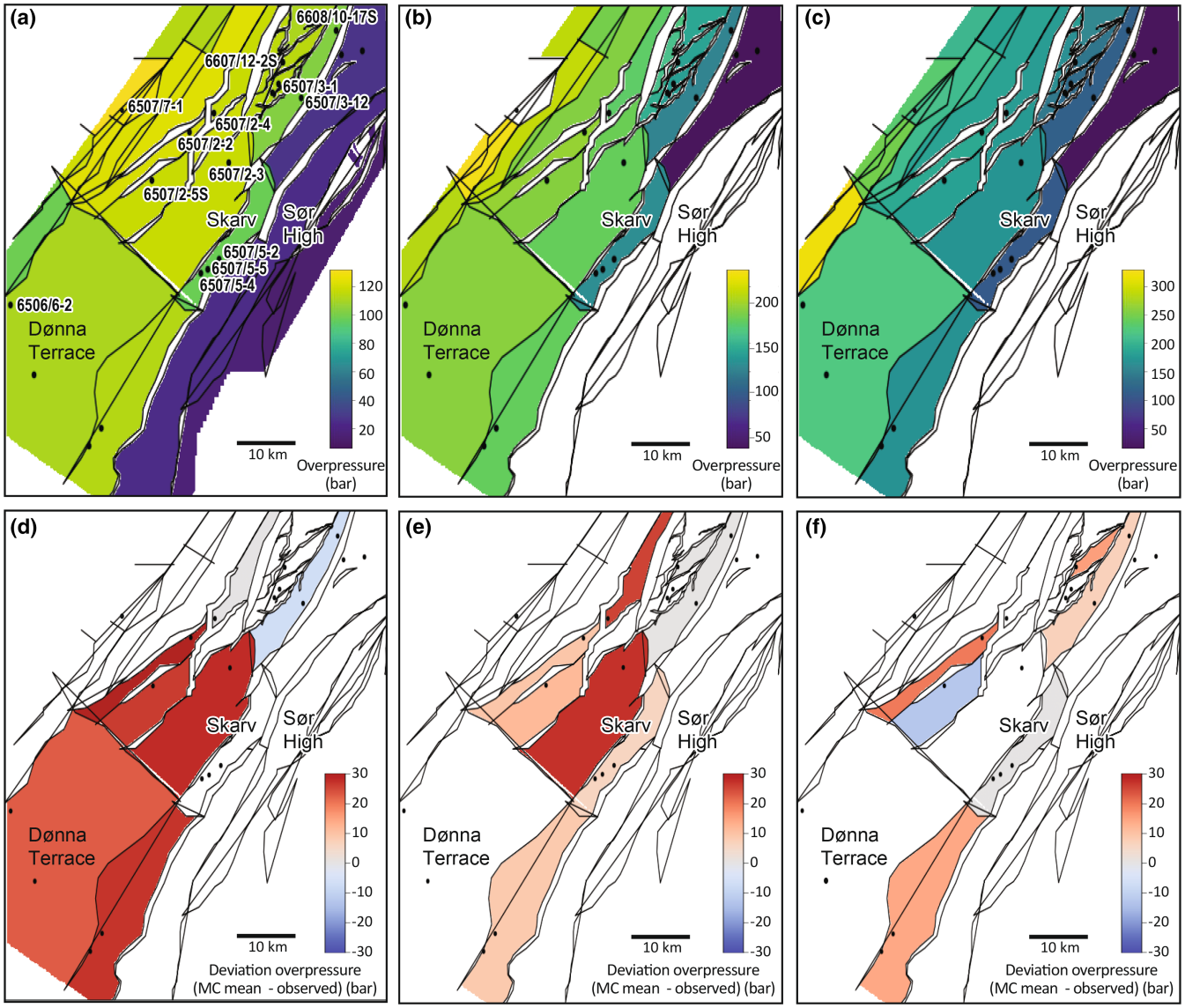

FIGURE 10 Simulated present-day overpressure for the study area for (a) Lysing Formation, (b) Intra Lange Fm. (reservoir #2) and (c) Intra Lange Fm (reservoir #3). Colour scale in bar. Deviation maps between modelled Monte Carlo mean and observed overpressures (bar) for (d) Lysing Formation (reservoir #1), (e) intra Lange Formation (reservoir #2), and (f) intra Lange Formation (reservoir #3).

But this sample has also a very low shale content, with Vsh 6%, indicating more a silty/sandy sample.

Figure 11b shows the corresponding simulated overpressures for the same runs and for the same pressure compartment. We do not have measured overpressure from the Lysing Formation. The simulated mean overpressure for the upper sandstone layer in the Lange Formation is 130 bar, while measured overpressures from well 6507/5-2 is 113–122 bar and 106–124 bar for well 6507/5-4 (reservoir #2 Lange Fm). For the deeper sandstone layer in the Lange Formation, the simulated overpressure is 130 bar, while the measured overpressures are 113–122 bar in well 6507/5-2 and between 120 bar to 148 bar in well 6507/5-4 (see range in measured overpressures for the compartment marked as a blue line in Figure 11b).

The simulated smectite content in the 1000 simulation runs for the Skarv pressure compartment (see Figure 1), can be compared with clay fraction XRD analysis from well 6507/5-4 (Skarv Field), and wildcat well 6507-11S situated south of our study area, see Figure 1 for location. Figure 12a,d show the simulated smectite content when the kinetic model from Huang et al. (1993a) is implemented in the 3D simulator, and the input parameter is varied as shown in Table 4. For Skarv compartment, we simulate a gradually reduction in smectite content from around 50% at 2.5 km depth, till around 10% smectite at 3.1 km depth (Figure 12a). We see the same overall trend from the XRD analysis for the well 65,075-4 in the same compartment, except some peaks of higher smectite fraction at around 3250 m

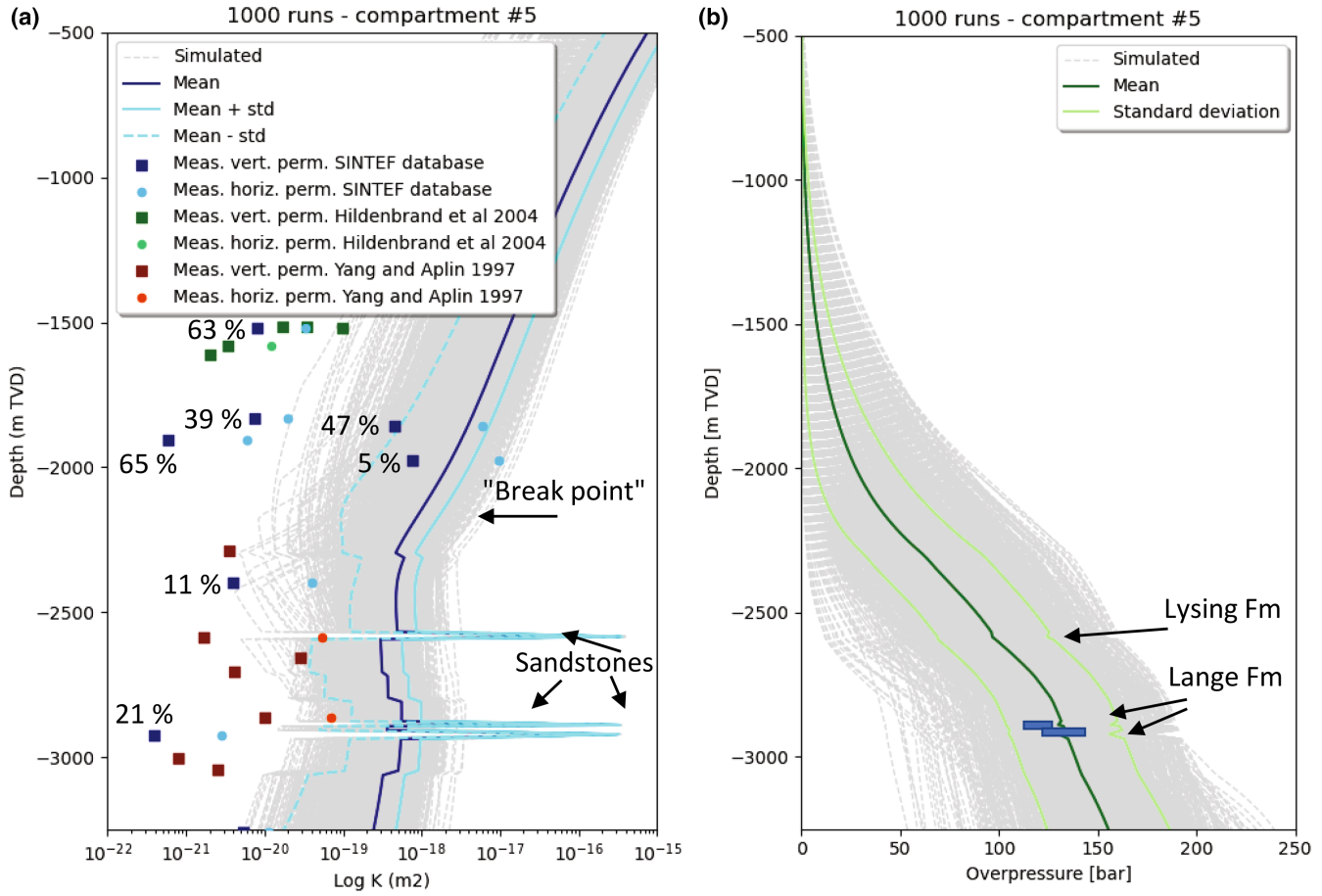

FIGURE 11 (a) Simulated log permeability versus depth (m TVD) for Skarv Field pressure cell with 1000 realizations. Mean simulated permeabilities with one standard deviation is marked. The simulated shale and sand permeabilities are compared to measured vertical and horizontal permeabilities from North Sea cores. Data from SINTEF in-house database, from Norwegian margin, Hildenbrand et al. (2004) and from the North Sea, Yang and Aplin (2007). For the own shale samples, the smectite + ML percent content is plotted. (b) Corresponding simulated overpressures versus depth for the 1000 realizations varying the input parameters, with mean overpressure and one deviation plotted. Magnitude of measured overpressures observed for the Skarv pressure cell is shown in blue. No data from Lysing Fm was available.

burial depth in well 6507/5-4 and around 2950 m and 3050 m TVD in well 6507/11-11S (Figure 12b,e). Cicchino et al. (2015) commented that some few samples clearly were contaminated by drilling mud, and therefore should be ignored, and that the smectite content decreased in all wells to values below 20%.

Figure 12c,f show the corresponding back-calculated smectite fraction to match the present measured smectite content. We see good match in the shallow part, for both wells (Figure 12c,f), but depths with high smectite contents are difficult to match, but as stated above, this is probable due to artefact of the drilling mud.

5 | DISCUSSION

One of the key processes in shales deposits is the smectite- illite conversion, where we in this work have implemented the Huang et al. (1993a) experimental derived kinetic model. Huang et al. (1993a) found that the potassium concentration varied typically in the range of 0.0026–0.0052 mol/L for oil field brines based on a large variety of geological settings (i.e. the Gulf of Mexico, Vienna Basin, Salton Trough, Taiwan Basin, Huasna Basin etc.). Bazin et al. (1997) show composition for oil field brines in the Greater Alwyn area, North Sea area varying from 0.00167 to 0.00524. Figure 2 showed that the potassium concentration has a larger effect with low heating rates in a sedimentary basin (e.g. Figure 2d with 1°C/My). With higher heating rates the effect is moderate to low. For simplification, we assume a constant rate of 0.0035 mol/L for the potassium concentration in the rest of the simulations.

One of the main assumptions we made, based on Bjørlykke and Nadeau (1998) and data from Pallatt et al. (1984) and de Waal et al. (1988), is that an exponential reduction in permeability is associated with the illite content. We assumed that a correction should be linked to the smectite-illite content, around a smectite factor of 0.8 (see Figure 3).

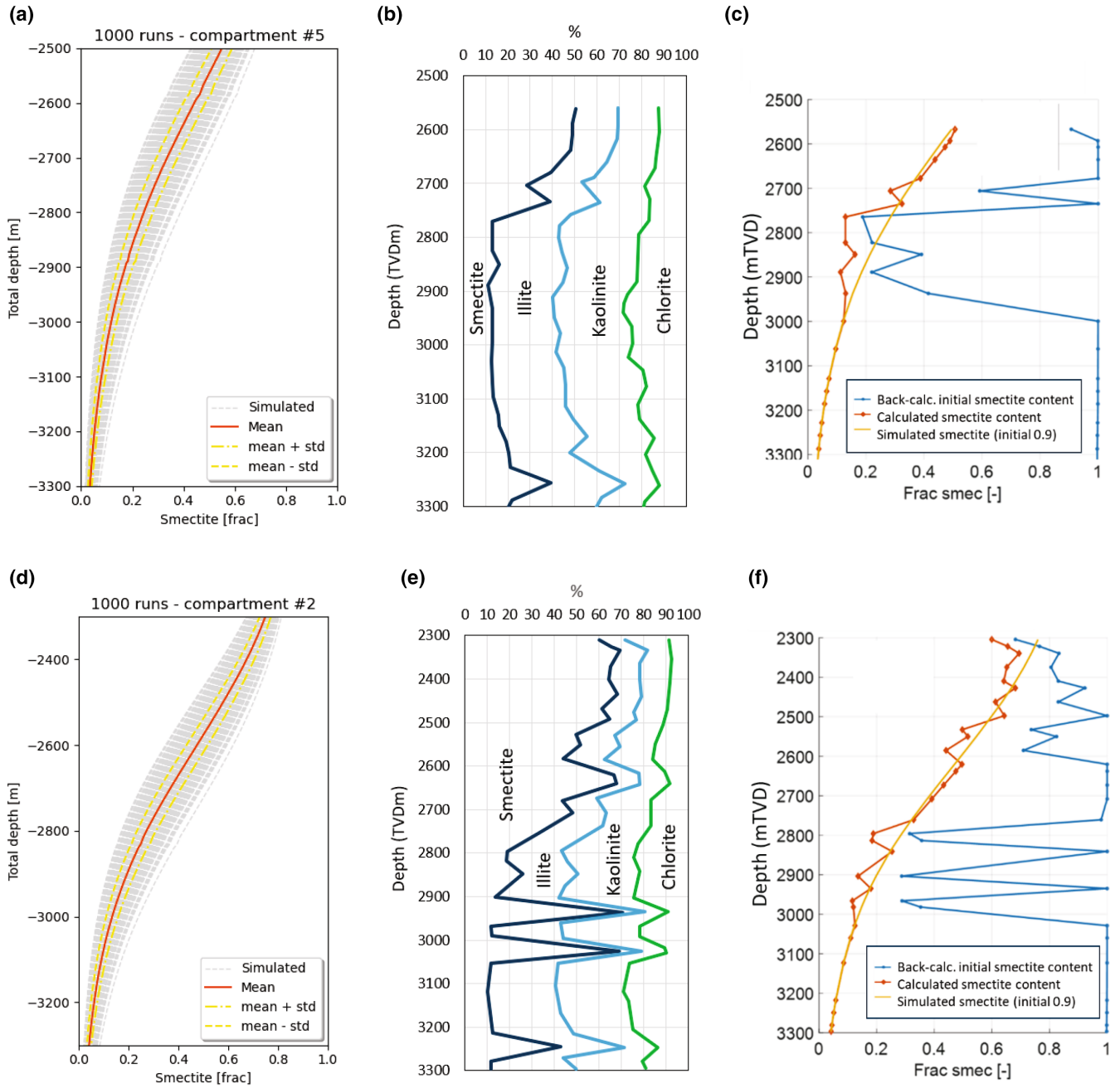

FIGURE 12 Variation in smectite fraction for 1000 runs for pressure compartments with (a) Skarv well 6507/5-4 and (d) well 6507/7-11S. (b and e) Clay fraction XRD analysis results for well 6507/5-4 and 6507/7-11S. Reworked from Cicchino et al. (2015). (c and f) Back-calculated initial smectite fraction (blue graph), red graph shows corresponding modelled best fit compared to observed present day smectite content, and orange graph shows modelled present day smectite content versus depth using an initial fraction of 0.9.

Nadeau et al. (2002) linked the increase in proportions of illite, intersecting clay-mineral packets and increasing overpressures. Andras (2018) showed, based on data from Lower Cretaceous mudstones from offshore Mid-Norway, Miocene mudstones from the Malay Basin and Triassic mudstone from Central North Sea, how the fabric alignment in the shales increase depending on burial depth starting from around 2000 m depth below the seafloor. The strong fabric alignment increases with chemically enhanced mechanical compaction. The same trend is seen from central Junggar Basin (China), but at larger burial depths (4000–4800 m), and temperatures of 90–105°C (Li et al., 2022). For this basin, we see even clearer the abrupt change in diagenesis with chemically enhanced compaction starts at around 20% illite in illite-smectite content. Thus, we clearly see from Figure 7a,d,g, that varying the *SIxs* parameter with Gaussian distribution 0.8 ± 0.08, keeping the rest of the input parameters constant, results in a spread in simulated shale permeabilities at shallow depth (< 2500 mTVD), and thereby variation in the start of

the overpressure ramp. Figure 7g shows a rapid pressure build-up of around 2.2 km ± 100 m. varying *SIzs* results in a deeper ramp, starting around 2.5 km depth ±100 m (Figure 7h), while *SIz*0 have minimal effect on the pressure ramp (Figure 7i).

5.1 | Smectite content

In our 3D pressure simulations, the initial smectite fraction (of shale content) is kept constant for all Monte Carlo runs and with a uniform value of 0.9 for all layers. This is a simplification and is probably not the case in the reality. Bjørlykke (2014) refer to depositional environment, provenance and climate as factors controlling rock properties at depths. In dry climates, there is less feldspar dissolution and precipitation of kaolinite, while in humid climates does fluvial and deltaic clays and silty mudstones have high content of kaolinite. Distal clays and deep-water clays are fine-grained with high content of smectite and illite and little kaolinite (Bjørlykke, 2014). Increased smectite content can also be a result of volcanic activity or reworked volcanic materials. To evaluate our simulation approach, we compared simulated smectite fraction in 1000 runs with measured XRD analysis from two wells, well 6507/5-4 from the Skarv area, and well 6507/7-11S situated 4 km south of the study area (see location on Figure 1). We see good match in the shallow parts, for both wells (Figure 12c,f), but depths with high smectite contents are difficult to match. Thus, from Cicchino et al. (2015) comment, these peaks are probable artefacts from drilling mud. Overall, an initial fraction of 0.9 in smectite, gives a good upscaling of the overall smectite fraction.

5.2 | Upscaling of shale permeabilities

To be able to simulate effect of smectite-illite transition on overpressure, it is important to have a good understanding and knowledge of the shale permeability. It is difficult and time-consuming to measure shale permeabilities in the laboratory, it is also challenging to get hold of high-quality specimens that are needed for such measurements due to the cost and few cores that are collected. Some studies have been carried out on synthetic samples. Mondol et al. (2007) generated brine-saturated clay slurries of smectite and kaolinite and measured smectite aggregates from 0.004 to 0.00006 mD (60 nD) at stresses between 1 MPa and 50 MPa. The SINTEF database from the North Sea presented in this work, carried out using transient pulse decay method, show measured permeabilities with different magnitude, varying from 10^{-18} to 10^{-22} m^2. Especially the shale samples from the shallow burial depths, from 1500 to 2000 m, show a large spread in measured permeability data. The shallow low permeability shales are in line with measured data from Palaeocene to Eocene shales from Norwegian margin (Hildenbrand et al., 2004). At depths >2 km, Yang and Aplin (2007) carried out extensive measurements using transient pulse decay technique on deeply buried mudstones from the North Sea resulting in a range from of measured vertical permeabilities from $8.0{\cdot}10^{-22}$ to $2.9{\cdot}10^{-22}$ m^2, the same order of magnitude as the SINTEF database at these depths.

All three shows higher measured permeabilities horizontally, compared to vertically. Ratio between vertical and horizontal permeability on samples are in range of one order of magnitude, probable due to sedimentological heterogeneities and layering within shales. Figure 11 shows clearly that the measured permeabilities from shales in the North Sea overall have lower permeability that the simulated permeabilities. Generally, the simulated permeabilities are two orders of magnitudes higher than the measured permeabilities. The measured permeabilities can be seen as "end members", how sealing the shales can be with no tracks or flaws, or sedimentary variations. When upscaling to hundreds for meters, one would not expect perfect tight shales, but also heterogeneities (silt and sands), cracks etc. Hantschel and Kauerauf (2009) suggest using a scaling factor of 0.01 for shales and using a Kozeny–Carman approach for basin modelling studies. However, on Figure 11a, we have included the percent of measured smectite + mixed layer for the samples tested at SINTEF. We see clearly from Table 4, and Figure 11a that the samples with high smectite/mixed layer content have low permeability at shallow depths. The exception in sample G, with low shale content. Using the simulation approach presented in this work, we are able to mimic the effect of smectite-illite transition and correction on the shale permeability beyond using two magnitudes scaling factor.

5.3 | Overpressure build-up

As mentioned in the introduction, velocity and density log data from Storvoll et al. (2005), shows low velocity interval in mudstones for the eastern Haltenbanken. This trend is line with our study area, with low velocities observed for the lower Miocene to upper Pliocene Kai Formation and the lower Eocene to lower Miocene Brygge Formation, with an abrupt reduction in the velocities from the overlying Quaternary Naust Formation. A question is if the low velocity is caused by overpressure or other factors. Hermanrud and Undertun (2019) suggest that since Brygge Formation and the Kai Formation are known to contain large amount of biogenic

silica (ooze) in the Norwegian Sea (e.g. Riis et al., 2005), the high silica content of biogene origin should explain the low velocities and densities. Thus, the appearance of these rocks could often be mistaken grey shales (with no biogenic material, and as rocks in compaction disequilibrium). This is in line with our simulations, where the overpressures gradually start to increase from around 1000 m, but the ramp structure, because of the smectite-illite transformation is simulated to take place from around 2200 m depth.

Build-up of overpressures are commonly associated with temperatures above about 100–120°C (e.g. Nadeau et al., 2002), where active mineral reactions in shales results in permeability reduction that are needed for overpressure to occur. The clay mineral reactions that release significant amounts of silica are smectite to mixed layer illite/smectite and illite and kaolinite to illite. These occurs at temperatures of 60–100°C and 120–140°C (e.g. Bjørlykke, 1998). Formation of small illite crystals from smectite or kaolinite are suggested to be the controlling mechanisms for permeability reduction (e.g. Freed & Peacor, 1989; Nadeau et al., 2002). Thyberg et al. (2010) points to that micro-quartz are the most probably sources from silica released during the smectite to illite dissolution-precipitation reaction. They also indicate that the released silica has not been exported out of the mudstones. Thus, the micro-quartz cementation process causes a significant change in mudstone stiffness and change in facies close to 2400–2600 m/70–90°C in Late Cretaceous mudstones offshore Norway (Thyberg et al., 2010). This is in line with our modelling, with permeability reduction around 2.4–2.5 km depth (Figure 11a), that is simulated as pressure build up. Since there exists no good methodology for direct measurement of the overpressures is shales, we have compared the simulated pore pressures in Lysing and Lange Formations sandstone units from RFT and FIT. We see from the deviation maps, good correlations in northern and western part of the study area, and better for the Lange Formation, then the shallower Lysing Formation (Figure 10). One explanation can be that the interpreted fault pattern at middle Jurassic top Garn Formation level, e.g. at deeper stratigraphic level, give too large modelled influence on the lateral flow pattern at Cretaceous level. However, if we examine the simulated pressure ramp build-up for the compartment at Skarv area, we see that for Lysing Fm., the mean overpressure is 96 ± 28 bar, thus the deviation is in the same range as one deviation. We see the presented methodology as a first step to better understand and simulated the diagenesis role and influence on pressure build-ups in shales. With increased lateral mapping and understanding of the smectite-illite distribution on the shale deposits, more detailed simulations can be evaluated in the future.

6 | CONCLUSIONS

- In this work we have been able to simulate a shallow overpressure build-up ramp in shales due to smectite-illite transition, using a kinetic approach. A permeability correction factor depending on the smectite-illite content has been introduced, assuming the main effect on shale permeabilities with a mixture of smectite-illite around 80% smectite fraction.
- The workflow including smectite-illite transition was tested in 1D simulations, concluding that heat flow and potassium content have impact on the smectite-illite transition. Thus, it was concluded that the potassium content can be assumed to be constant in warmer basins. With low heat-rate (1 C/My), the potassium concentration should be considered.
- Simulated shale permeabilities are two orders of magnitude higher than measured shale permeabilities from the lab. The samples measured in the lab are "end-members" with low permeabilities and no fractures or cracks, while the upscaled permeabilities averaging over hundreds of meters should be higher in magnitude.
- Permeabilities have been measured using transient decay methods for shales and different burial depths from North Sea samples. The measured permeabilities are in range of $2.66 \cdot 10^{-18}$ to $3.94 \cdot 10^{-22}\,m^2$, and in the same range as published data from Yang and Aplin (2007) and Hildenbrand et al. (2004). The XRD analysis from the shale samples showed high smectite and mixed layer content for all the shallow buried shales, with low permeability.
- Results from the 3D case study with the smectite-illite transition included for the shale permeability simulations, indicate that including these effects can help understanding and predicting the onset of pressure ramps (transition from hydrostatic to overpressure conditions) as well as overall pressure distribution within a sedimentary basin. Work remains for ranking the effect of smectite-illite transformation with other processes with large uncertainties like e.g. fault transmissibilities, detailed knowledge of smectite-illite variation laterally and vertically.

ACKNOWLEDGEMENTS

We would like to thank The Norwegian Research Council and AkerBP, Wintershall, ConocoPhillips and Equinor for funding the knowledge building project: "Reduced uncertainty in overpressures and drilling window prediction ahead of the bit (PressureAhead)" 255418/E30. We would also like to thank AkerBP for input data and for funding the "Pilot field test PressureAhead" project, and Vår Energy for funding "PressureAhead Extension". Berit Fossum has helped with drawing of some of the figures.

CONFLICT OF INTEREST STATEMENT

There is no conflict of interest.

PEER REVIEW

The peer review history for this article is available at https://www.webofscience.com/api/gateway/wos/peer-review/10.1111/bre.12815.

DATA AVAILABILITY STATEMENT

The data that support the findings of this study are available from AkerBP and SINTEF Industry. Restrictions apply to the availability of these data, which were used under license for this study. Data are available from the author(s) with the permission of AkerBP and SINTEF Industry.

REFERENCES

Andras, P. (2018). *The role of clay mineral diagenesis in overpressure generation and compaction of siliciclastic mudstones*. Doctoral Dissertation PhD thesis. University of Durham.

Bazin, B., Brosse, E., & Sommer, F. (1997). Chemistry of oil-field brines in relation to diagenesis of reservoirs—2. Reconstruction of palaeo-water composition for modelling illite diagenesis in the greater Alwyn area (North Sea). *Marine and Petroleum Geology*, *14*(5), 497–511.

Bjørlykke, K. (1998). Pore-water flow and mass transfer of solids in solution in sedimentary basins. In A. Parker & B. W. Sellwood (Eds.), (pp. 189–221). Quantitative Diagenesis: Recent Developments and Applications to Reservoir Geology.

Bjørlykke, K. (2014). Relationships between depositional environments, burial history and rock properties. Some principal aspects of diagenetic process in sedimentary basins. *Sedimentary Geology*, *301*, 1–14.

Bjørlykke, K., & Nadeau, P. H. (1998). Temperature controlled porosity/permeability reduction, fluid migration, and petroleum exploration in sedimentary basins. *Australian Petroleum Production & Exploration Association Journal*, *38*, 453–464.

Blystad, P., Brekke, H., Færseth, R. B., Larsen, B. T., Skogseid, J., & Tørudbakken, B. (1995). Structural elements of the Norwegian continental shelf. Part II the Norwegian Sea region. *Norw. Pet. Dir. Bull.*, *8*, 45.

Borge, H. (2000). *Fault controlled pressure modelling in sedimentary basins*. PhD thesis. Norwegian University of Science and Technology.

Borge, H., & Sylta, Ø. (1998). 3D modelling f fault bounded pressure compartments in the North Viking Graben. *Energy, Exploration and Exploitation*, *16*, 301–323.

Brekke, H., Dahlgren, S., Nyland, B., & Magnus, C. (1999). The prospectivity of the Vøring and Møre basins on the Norwegian Sea continental margin. In A. Fleet & S. Boldy (Eds.), *Petroleum geology of Northwest Europe: Proceedings of the fifth conference* (Vol. *5*, pp. 261–274). The Geological Society of London.

Casciello, E., Cosgrove, J. W., Cesarano, M., Romero, E., Queralt, I., & Vergés, J. (2011). Illite-smectite patterns in sheared Pleistocene mudstones of the southern Apennines and their implications regarding the process of illitization: A multiscale analysis. *Journal of Structural Geology*, *33*, 1699–1711.

Chand, S., Rise, L., Knies, J., Haflidason, H., Hjelstuen, B. O., & Bøe, R. (2011). Stratigraphic development of the south Vøring margin (mid-Norway) since early Cenozoic time and its influence on subsurface fluid flow. *Marine and Petroleum Geology*, *28*, 1350–1363.

Cicchino, A. M. P., Sargent, C., Goulty, N. R., & Ramdhan, A. M. (2015). Regional variation in cretaceous mudstone compaction trends across Haltenbanken, offshore mid-Norway. *Petroleum Geoscience*, *21*(1), 17–34.

Colten-Bradley, V. A. (1987). Role of pressure in smectite dehydration – Effects on geopressure and smectite-to-illite transformation. *American Association of Petroleum Geologists Bulletin*, *71*(11), 1414–1427.

Crawford Elliott, W., & Matisoff, G. (1996). Evaluation of kinetic models for the smectite to illite transformation. *Clays and Clay Minerals*, *44*(1), 77–87.

Daigle, H., & Screaton, E. J. (2015). Evolution of sediment permeability during burial and subduction. *Geofluids*, *15*, 84–105.

Dalland, A., Wosley, D., & Ofstad, K. (1988). A lithostratigraphic scheme for the Mesozoic and Cenozoic succession offshore mid and northern Norway. *Norwegian Petroleum Directorate Bulletin*, *4*, 65.

de Waal, J. A., Bil, J. K., Kantorowicz, J. D., & Dicker, A. I. M. (1988). Petrophysical core analysis of sandstones containing delicate illite. *Log Analyst*, *29*, 317–331.

Dewhurst, D. N., Yang, Y., & Aplin, A. C. (1999). Permeability and fluid flow in natural mudstones. *Geological Society, London, Special Publications*, *158*, 23–43.

Eidvin, T., Bugge, T., & Smelror, M. (2007). The Molo formation, deposited by coastal progradation on the inner mid-Norwegian continental shelf, coeval with the Kai formation to the west and the Utsira formation in the North Sea. *Norw. Jour. Geol.*, *87*, 35–102.

Færseth, R. B., & Lien, T. (2002). Cretaceous evolution in the Norwegian Sea – A period characterized by tectonic quiescence. *Marine and Petroleum Geology*, *19*(8), 1005–1027.

Freed, R. L., & Peacor, D. R. (1989). Geopressured shale and sealing effect of smectite to illite transition. *The American Association of Petroleum Geologists Bulletin*, *73*(10), 1123–1232.

Grauls, D. (1998). Overpressure assessment using a minimum principal stress approach. *Overpressures in petroleum exploration. Workshop proceedings in petroleum exploration*, Pau (France), 7–8 April. Elf Exploration Production, Centre Scientifique et Technique.

Grøver, A., Roli, O.-A., & Lothe, A. E. (2018). New methodology for 3D geo-pressure modelling with multi burial and uplift effects. *Poster at AAPG ICE*, South Africa, December 2018.

Hansen, L. A. S., Hodgson, D. M., Pontén, A., Thrana, C., & Obradors Latre, A. (2021). Mixed axial and transverse deep-water systems: The cretaceous post-rift lysing formation, offshore Norway. *Basin Research*, *33*, 2229–2251.

Hantschel, T., & Kauerauf, A. I. (2009). *Fundamentals of basin and petroleum systems modeling*. Springer-Verlag.

Harrison, W. J., & Summa, L. L. (1991). Paleohydrology of the Gulf of Mexico Basin. *American Journal of Science*, *291*, 109–176.

Helset, H. M., Lander, R. H., Matthews, J. C., Reemst, P., et al. (2002). The role of diagenesis in the formation of fluid overpressures in clastic rocks. *Hydrocarbon Seal Quantification Norwegian Petroleum Society Special Publications*, *11*, 37–50.

Hermanrud, C., & Undertun, O. (2019). Resolution limits of fluid overpressures from mineralogy, porosity, and sonic velocity variations in North Sea mudrocks. *AAPG Bulletin*, *103*(11), 2665–2695.

Hildenbrand, A., Schlomer, S., Krooss, B. M., & Littke, R. (2004). Gas breakthrough experiments on pelitic rocks: Comparative study with N2, CO2 and CH4. *Geofluids*, *4*, 61–80.

Horsrud, P., Sønstebø, E. F., & Bøe, R. (1998). Mechanical and petrophysical properties of North Sea shales. *Int. J. of Rock Mech. Min. Sci.*, *35*(8), 100–1020.

Hower, J., Eslinger, E. V., Hower, M. E., & Perry, E. A. (1976). Mechanism of burial metamorphism of argillaceous sediment: 1. Mineralogical and chemical evidence. *GSA Bulletin*, *87*(5), 725–737.

Huang, W.-L., Longo, J. M., & Pevear, D. R. (1993a). An experimentally derived kinetic model for smectite-to-illite conversion and its use as a geothermometer. *Clay and Clay Minerals*, *41*(2), 162–177.

Huang, W. L., Longo, J. M., & Pevear, D. R. (1993b). Erratum to: An experimentally derived kinetic model for smectite-to-illite conversion and its use as a geothermometer. *Clays and Clay Minerals*, *41*, 770. https://doi.org/10.1346/CCMN.1993.0410617

Kim, J., Dong, H., Seabaugh, J., Newell, S. W., & Eberl, D. D. (2004). Role of microbes in the smectite-to-illite reaction. *Science*, *303*, 830–832.

Kim, J., Dong, H., Yang, K., Park, H., Elliott, W. C., Spivack, A., Koo, T. H., Kim, G., Morono, Y., Henkel, S., Inagaki, F., Zeng, Q., Hoshino, T., & Heuer, V. B. (2019). Naturally occurring, microbially induced smectite-to-illite reaction. *Geology*, *47*, 535–539.

Lahann, R. W., & Swarbrick, R. E. (2011). Overpressure generation by load transfer following shale framework weakning due to smectite diagenesis. *Geofluids*, *11*, 362–375.

Li, C., Zhang, L., Luo, X., Zeng, X., Xiu, J., Lei, Y., Cheng, M., Hu, C., Zhang, M., & He, W. (2022). Clay mineral transformations of Mesozoic mudstones in the central Junggar Basin, northwestern China: Implications for compaction properties and pore pressure responses. *Marine and Petroleum Geology*, *144*, 105847.

Lothe, A. E. (2004). *Simulations of hydraulic fracturing and leakage in sedimentary basins*, Ph.D. thesis. University of Bergen.

Lothe, A. E., Borge, H., & Gabrielsen, R. H. (2004). Modelling of hydraulic leakage by pressure and stress simulations: An example from the Halten terrace area, offshore mid-Norway. *Petroleum Geoscience*, *10*(3), 199–213.

Lothe, A. E., Cerasi, P., & Aghito, M. (2019). Digitized uncertainty handling of pore pressure and mud-weight window ahead of bit: North Sea example. *SPE Journal*, *25*, 529–540.

Lothe, A. E., Grøver, A., Roli, O.-A., Cerasi, P., Skogestad, J.-O., Kristiansen, T. G., Bauer, A., Guida, A., & Boukili, M. (2020). Pilot field trial of real-time pore pressure and well stability updates in a digital twin coupling. *Third EAGE Workshop on Pore Pressure Prediction*, 6–7 December 2020, Amsterdam, the Netherlands, Extended abstract.

Lothe, A. E., Grøver, A., Roli, O. A., Stenebråten, J., & Kristiansen, T. G. (2022). Upscaling of shale permeabilities from lab to basin scale 3D pressure modelling using a stochastic approach. *6th International Workshop on Rock Physics*, A Coruna, Spain, 13–17 June 2022, Extended abstract.

Mondol, N. H., Bjørlykke, K., Jahren, J., & Høeg, K. (2007). Experimental mechanical compaction of clay mineral aggregates-changes in physical properties of mudstones during burial. *Marine and Petroleum Geology*, *24*, 289–311.

Mondol, N. H., Fawad, M., Jahren, J., & Bjørlykke, K. (2008). Synthetic mudstone compaction trends and their use in pore pressure prediction. *First Break*, *26*, 43–51.

Nadeau, P. H., Peacor, D. R., Yan, J., & Hillier, S. (2002). I-S precipitation in pore space as the cause of geopressuring in Mesozoic mudstones, Egersund Basin, Norwegian continental shelf. *American Mineralogist*, *87*, 1580–1589.

Nadeau, P. H., & Reynolds, R. C. (1981). Burial and contact metamorphism in the Mancos shale. *Clays and Clay Minerals*, *29*, 249–259.

Nguyen, B. T., Kido, M., Okawa, N., Fu, H., Kakizaki, S., & Imahori, S. (2016). Compaction of smectie-rich mudstone and its influence on pore pressure in the deepwater Joetsu Basin, Sea of Japan. *Marine and Petroleum Geology*, *78*, 848–869.

Nooraiepour, M., Mondol, N. H., & Hellevang, H. (2019). Permeability and physical properties of semi-compacted fine-grained sediments – A laboratory study to constrain mudstone compaction trends. *Marine and Petroleum Geology*, *102*, 590–603.

O'Connor, S., Swarbrick, R., & Jones, D. (2008). Where has all the pressure gone? Evidence from pressure reversals and hydrodynamics. *First Break*, *26*, 55–61.

Osborne, M. J., & Swarbrick, R. (1997). Mechanics for generating overpressure in sedimentary basins: A reevaluation. *AAPG Bulletin*, *81*, 1023–1041.

Pallatt, N., Wilson, M. J., & McHardy, W. J. (1984). The relationship between permeability and the morphology of diagenetic illite in reservoir rocks. *Journal of Petroleum Technology*, *36*, 2225–2227.

Peltonen, C., Marcussen, Ø., Bjørlykke, K., & Jahren, J. (2009). Clay mineral diagenesis and quartz cementation in mudstones: The effects of smectite to illite reaction on rock properties. *Marine and Petroleum Geology*, *26*, 887–898.

Powers, M. C. (1967). Fluid-release mechanisms in compacting marine mudrocks and their importance in oil exploration. *The American Association of Petroleum Geologists Bulletin*, *51*(7), 1240–1254.

Pytte, A. M. (1982). *The kinetics of the smectite to illite reaction in contact metamorphic shales*. Master Thesis. Dartmouth College, Hanover, NH.

Pytte, A. M., & Reynolds, R. C. (1989). The thermal transformation of smectite to illite. In N. D. Naeser & T. H. McCulloh (Eds.), *Thermal transformation of smectite to illite* (pp. 133–140). Springer-Verlag.

Riis, F., Berg, K., Cartwright, J., Eidvin, T., & Hansch, K. (2005). Formation of large, craterlike evacuation structures in ooze sediments in the Norwegian Sea. Possible implications for the development of the Storegga slide. *Marine and Petroleum Geology*, *22*, 257–273.

Rise, L., Ottesen, D., Berg, K., & Lundin, E. (2005). Large-scale development of the mid-Norwegian margin during the last 3 million years. *Marine and Petroleum Geology*, *22*, 33–44.

Sclater, J. G., & Christie, P. A. F. (1980). Continental stretching: An explanation of the post-mid cretaceous subsidence of the Central North Sea basin. *Journal of Geophysical Research*, *85*(B7), 243–253.

Storvoll, V., Bjørlykke, K., & Mondol, N. H. (2005). Velocity-depht trends in Mesozoic and Cenozoic sediments form the Norwegian shelf. *AAPG Bulletin*, *89*(3), 359–381.

Strout, J. M., & Tjelta, T. I. (2007). Excess pore pressure measurement and monitoring for offshore instability problems. *Presentation at Offshore Technology Conference*, Houston, TX, 30 April–3 May 2007. OTC paper 18706.

Swarbrick, R. E., Osborne, M., & Yardley, G. S. (2002). Comparison of overpressure magnitude resulting from the main generating mechanisms. In A. R. Huffman & G. L. Bowers (Eds.), *Pressure regimes in sedimentary basins and their predictions* (Vol. *76*, pp. 1–12). AAPG Memoir.

Thyberg, B., Jahren, J., Winje, T., Bjørlykke, K., Faleide, J. I., & Marcussen, Ø. (2010). Quartz cementation in late cretaceous mudstones, northern North Sea: Changes in rock properties due to dissolution of smectite and precipitation of micro-quartz crystals. *Marine and Petroleum Geology*, *27*, 1752–1764.

van der Pluijm, B. (2011). Natural fault lubricants. *Nature Geoscience*, *4*, 217–218.

Velde, B., & Vasseur, G. (1992). Estimation of the diagenetic smectite-to-illite transformation in time-temperature space. *Am. Minearl*, *77*, 967–976.

Walderhaug, O. (1996). Kinetic modeling of quartz cementation and porosity loss in deeply buried sandstone reservoirs. *American Association of Petroleum Geologists Bulletin*, *80*(5), 731–745.

Wensaas, L., Shaw, H. F., Gibbons, K., Aagaard, P., & Dypvik, H. (1994). Nature and causes of overpressuring in mudrocks of the Gullfaks area, North Sea. *Clay Minerals*, *29*, 439–449.

Yang, Y., & Aplin, A. (1998). Influence of lithology and compaction on the pore size distribution and modelled permeability of some mudstones from the Norwegian margin. *Marine and Petroleum Geology*, *15*(2), 163–175.

Yang, Y., & Aplin, A. C. (2007). Permeability and petrophysical properties of 30 natural mudstones. *Journal of Geophysical Research B: Solid Earth*, *112*, B03206.

How to cite this article: Lothe, A. E., Grøver, A., Roli, O.-A., Stenebråten, J., & Kristiansen, T. G. (2023). Simulations of the effect of smectite-to-illite transition in shales on permeability and overpressures using a stochastic approach, a Norwegian margin case study. *Basin Research*, *00*, 1–25. https://doi.org/10.1111/bre.12815